

[Electronic Supporting Information to accompany]

Design, Synthesis, Characterization, and Catalytic Properties of a Large-pore MOF Possessing Single-site Vanadyl(monocatecholate) Moieties

Huong Giang T. Nguyen, Mitchell H. Weston, Amy J. Sarjeant, Daniel M. Gardner, Zhi An, Raanan Carmieli, Michael R. Wasielewski, Omar K. Farha,* Joseph T. Hupp,* and SonBinh T. Nguyen*

Department of Chemistry and International Institute for Nanotechnology, Northwestern University, 2145 Sheridan Road, Evanston, Illinois 60208-3113, USA

Table of Contents

S1. Materials and methods and synthesis of precursors and ligands	S1
S2. NMR spectra of ligands	S6
S3. Characterization data for PG-CatBrO-MOFs (single-crystal X-ray diffraction, photographic picture, EA, TGA, CO ₂ isotherms, NMR spectra), as well as characterization data for CatBrO MOF and V-CatBrO MOF (CO ₂ isotherms, NMR spectra, photographic pictures, FTIR spectra, PXRD patterns, TGA, ICP-OES, XPS spectra, and EPR spectra)	S16
S4. Catalysis-related data (control benzylic oxidation with BOC-CatBrO MOF, and PXRD data, TGA, and photographic pictures of V-CatBrO MOF after catalysis)	S34
S5. References	S35

S1. Materials and methods and synthesis of precursors and ligands

Materials and methods. Unless otherwise stated, all reagents were used as received. 1,3-dimethoxybenzene, *n*-butyl lithium, *N,N,N',N'*-tetramethylethylenediamine, chlorotrimethylsilane, iodine monochloride, boron tribromide, *tert*-butyldimethylsilyl chloride, imidazole, potassium carbonate, 4-(dimethylamino)pyridine, di-*tert*-butyl dicarbonate, 2-nitrobenzyl bromide, 4-ethynylpyridine hydrochloride, *tetrakis*(triphenylphosphine)palladium, copper(I) iodide, diisopropylamine, triethylamine, hexabromobenzene, 4-tolylmagnesium bromide, nitric acid, 1,4-diazabicyclo[2.2.2]octane (DABCO), vanadyl acetylacetonate, naphthalene, *tert*-butyl hydroperoxide (5-6 M in nonane), α -tetralone, 1,2,3,4-tetrahydro-1-naphthol, and aqueous hydrogen peroxide (30 wt %) were purchased from Aldrich Chemicals Company, Inc. (Milwaukee, WI). Concentrated sulfuric acid, sodium sulfate, and Celite were purchased from VWR Scientific, LLC (Chicago, IL). Vanadium, silicon, and zinc ICP standards were purchased from Sigma-Aldrich (St. Louis, MI). Magnesium sulfate was purchased from Mallinckrodt Baker, Inc. (Phillipsburg, NJ). Sodium bisulfite and 1,2-dichlorobenzene were purchased from Fisher Scientific, Inc. (Pittsburg, PA). Bromine was purchased from Alfa Aesar (Ward Hill, MA). 1,2,3,4-Tetrahydronaphthalene was purchased from TCI America (Portland, OR). Ultrapure deionized water (18.2 M Ω •cm resistivity) was obtained from a Millipore Milli-Q Biocel A10 instrument (Millipore Inc., Billerica, MA). Solvents were purchased from either Sigma-Aldrich (St. Louis, MI) or Fisher Scientific, Inc. (Pittsburg, PA). Dry solvents were prepared by passing HPLC-grade solvents through a Dow-Grubbs solvent system installed by Glass Contours (now JC Meyer Solvent Systems, Laguna Beach, CA, USA). All dry solvents were collected under inert gases, degassed under vacuum, and stored under nitrogen in a Strauss flask prior to use.

Powder X-ray diffraction (PXRD) patterns were recorded on a Rigaku X-ray Diffractometer Model ATX-G (Tokyo, Japan) equipped with an 18 kW Cu rotating anode, an MLO monochromator, and a high-count-rate scintillation detector. Measurements were made over a range of $2^\circ < 2\theta < 30^\circ$ in 0.05° step width with a $2^\circ/\text{min}$ scanning speed.

Due to small amount of samples, powder patterns for photochemically deprotected ***o*NBn-CatBrO MOF** and **V-CatBrO MOF** after catalysis were collected on a Bruker AXS APEX2 diffractometer equipped with a CCD detector and a CuK α 1 μ S microfocus source with MX optics. Samples were loaded into glass capillaries with a small amount of mother liquor and mounted on a goniometer head. Data were collected with an area detector as rotation frames over 180° in ϕ at 2θ values of 12° degree offsets ranging from 12° to a maximum of 60° and exposed for 10 minutes for each frame. At a distance of 150 mm, the detector area covers 24° in 2θ . Overlapping sections of data were matched and the resulting pattern integrated using the Bruker APEX2 Phase ID program. Powder pattern data were treated for amorphous background scatter (EVA 16, Copyright Bruker-AXS 1996-2010).

Elemental analysis (CHN), was performed by Micro Analysis Inc. (Wilmington, DE, USA).

CO₂ adsorption and desorption isotherms were measured on either an Autosorb 1-MP instrument (Quantachrome Instruments, Boynton Beach, FL) or a Micromeritics Tristar II 3020 (Micromeritics, Norcross, GA) at 273K. Before each run, samples were solvent-exchanged to ethanol and activated under supercritical CO₂^{S1} or solvent exchanged to DCM. Residual solvent was removed at room temperature or 120 °C under high vacuum on a MasterPrep (Quantachrome Instruments, Boynton Beach, FL). Around 10-30 mg of sample was used in each measurement. All the gases used for the adsorption and desorption measurements were Ultra High Purity Grade 5 and were obtained from Airgas Specialty Gases (Chicago, IL).

Thermogravimetric analyses (TGAs) were performed on a Mettler Toledo TGA/DSC 1 Star^c System (Schwerzenbach, Switzerland) interfaced with a PC using Star^c software (version 9.10). Samples were placed in alumina pans and heated at a rate of 10 °C/min from 25-700 °C under a nitrogen atmosphere.

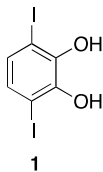
Fourier-transformed infrared (FTIR) spectroscopy was performed on a Thermo Nicolet Nexus 870 FTIR spectrometer (Thermo Scientific, Waltham, MA), using KBr pellets. Frequencies are given in reciprocal centimeters (cm⁻¹). The FTIR spectra were analyzed using EZ Omnic software (Thermo Scientific, Waltham, MA).

Inductively coupled plasma optical-emission spectroscopy (ICP-OES) was conducted on a Varian Vista-MDX model ICP-OES spectrometer (Varian, Walnut Creek, CA) equipped with a CCD detector and an argon plasma to cover the 175-to-785 nm spectral range. Samples (1-3 mg) were digested in a small amount (1 mL) of a mixture of 3:1 v/v conc. H₂SO₄:H₂O₂ (30 wt % in H₂O) by heating in a Biotage (Uppsala, Sweden) SPX microwave reactor (software version 2.3, build 6250) at 180 °C until the solution became clear. The acidic solution was diluted to 25 mL with ultrapure deionized H₂O and analyzed for V (292.401 and 309.310 nm), Si (185.005 and 212.412 nm), and/or Zn (213.857 and 202.548 nm) content as compared to standard solutions.

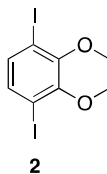
X-ray photoelectron spectroscopy (XPS) measurements were carried out at the KECK-II/NUANCE facility at NU on a Thermo Scientific ESCALAB 250 Xi (Al K α radiation, hv = 1486.6 eV) equipped with an electron flood gun. XPS data was analyzed using Thermo Scientific Avantage Data System software and all spectra were referenced to the C1s peak (284.5 eV). Porous samples were evacuated overnight before analysis.

Steady-state continuous-wave electron paramagnetic resonance (CW-EPR) spectra were measured using a Bruker Elexsys E580 X-Band EPR spectrometer with a Bruker EN 4118X-MD4 resonator. Microwave power was set to 2 mW and field modulation was set to 0.050 mT at 100 kHz. Dry compound and chlorobenzene solutions of the samples were loaded into quartz sample tubes (2 mm o.d. \times 1 mm i.d.) under ambient conditions and sealed with UV-curable epoxy prior to experiments. Temperature was maintained at 7.0 \pm 0.1 K.

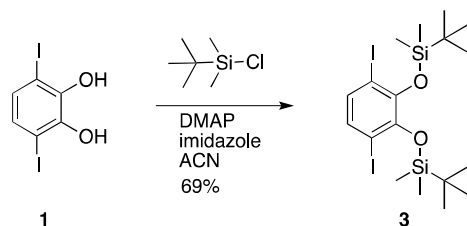
¹H and ¹³C NMR spectra were recorded on a Bruker 500 FT-NMR spectrometer (499.773 MHz for ¹H, 125.669 MHz for ¹³C). ¹H and ¹³C chemical shifts are reported in ppm from TMS with the residual solvent resonances as internal standards. In a typical MOF digestion, a sample (~ 5 mg) of MOF dried on filter paper was digested in a small amount (0.5 mL) of conc. D₂SO₄ or a mixture of conc. HCl/DMSO-*d*₆ (9:1 v/v)



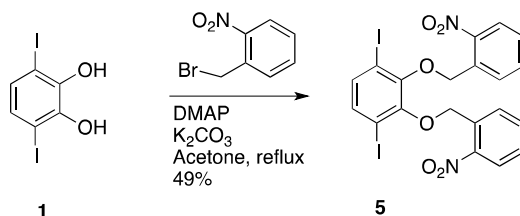
1,4-Diiodo-2,3-dihydroxybenzene (1). Compound **1** was synthesized according to a literature protocol.^{S2} ¹H NMR (500 MHz, CDCl₃, see Figure S1): δ 7.00 (s, 2H), 5.63 (s, 2H). ¹³C NMR (126 MHz, CDCl₃, see Figure S2): δ 143.1, 131.2, 83.5.



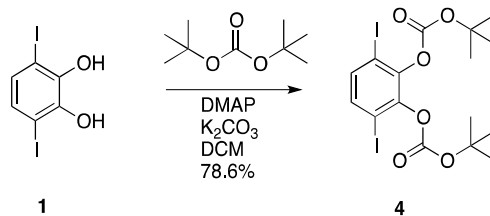
1,4-Diiodo-2,3-dimethoxybenzene (2). Compound **2** was synthesized according to a literature protocol.^{S2} ¹H NMR (500 MHz, CDCl₃, see Figure S3): δ 7.24 (s, 2H), 3.86 (s, 6H). ¹³C NMR (126 MHz, CDCl₃, see Figure S4): δ 153.2, 135.5, 93.0, 60.8.



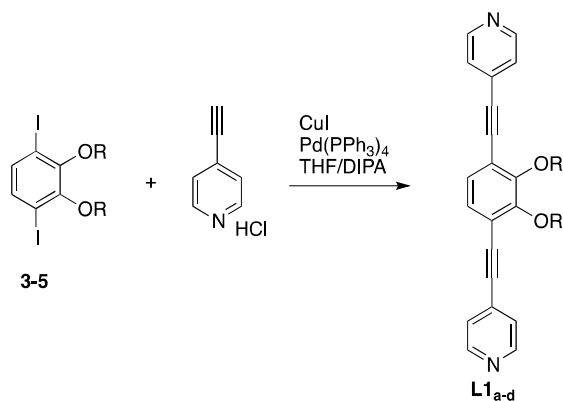
2,3-Bis(tert-butyldimethylsilyloxy)-1,4-diiodobenzene (3). 1,4-Diiodo-2,3-dihydroxybenzene (2 g, 5.53 mmol) was placed in a 250 mL Schlenk flask equipped with a magnetic stir bar. A catalytic amount of 4-(dimethylamino)pyridine was added. The flask was then subjected to three cycles of evacuation and N₂ refill. Anhydrous acetonitrile (25 mL) was added and the mixture was left to stir for 5 minutes. To the reaction flask was then added imidazole (0.83 g, 12.2 mmol) and *tert*-butyldimethylsilyl chloride (1.83 g, 12.2 mmol), and the resulting mixture was left to react for 8 h. TLC analysis, using a mixture of ethyl acetate/hexanes (1/1 v/v) as the eluent, indicated the presence of both mono- and di-protected products. Thus, additional imidazole (415 mg, 6.1 mmol), *tert*-butyldimethylsilyl chloride (916 mg, 6.1 mmol), and acetonitrile (20 mL) were added and the reaction was allowed to stir overnight. In the morning, the reaction mixture was filtered through a coarse-fritted funnel and then through a medium-grade Whatman filter paper to remove all insoluble by-products. The filtrate was then evaporated in vacuo to afford a brown solid that was then purified by flushing with hexanes through a plug of silica gel (6 × 12 cm). The eluted yellow fraction was then collected and evaporated to dryness to give a yellow product (2.25 g, 69% yield). ¹H NMR (500 MHz, CDCl₃, see Figure S5): δ 7.11 (s, 2H), 1.08 (s, 18H), 0.19 (s, 12H). ¹³C NMR (126 MHz, CDCl₃, see Figure S6): δ 147.9, 133.9, 92.9, 27.1, 25.9, 19.0.



1,4-Diiodo-2,3-bis((2-nitrobenzyl)oxy)benzene (4). 1,4-Diiodo-2,3-dihydroxybenzene (2 g, 5.52 mmol), 2-nitrobenzyl bromide (2.62 g, 12.2 mmol), K₂CO₃ (2.29g, 16.6 mmol), and 4-(dimethylamino)pyridine (136 mg, 1.11 mmol) were placed in a 100 mL round-bottom flask equipped with a magnetic stir bar. Acetone (50 mL) was added and the reaction mixture was refluxed at 80 °C overnight while stirring. In the morning, the content of the reaction was evaporated to dryness and the resulting solid was redissolved in a minimum amount of dichloromethane and filtered through celite. The filtrate was evaporated in vacuo and the resulting solid was purified via flash chromatography (10 vol % ethyl acetate in hexanes, 6 × 12 cm silica gel) to give a yellow product (1.7 g, 49% yield). ¹H NMR (500 MHz, CDCl₃, see Figure S7): δ 8.02 (m, 2H), 8.00 (m, 2H), 7.59 (dt, *J* = 7.7, 1.3 Hz, 2H), 7.37 (t, *J* = 7.8 Hz, 2H), 7.36 (s, 2H), 5.38 (s, 4H). ¹³C NMR (126 MHz, CDCl₃, see Figure S8): δ 151.8, 146.1, 136.3, 134.0, 133.6, 128.2, 128.1, 124.6, 93.0, 71.6.



1,4-Diiodobenzene-2,3-bis(*tert*-butoxycarbonyloxy)benzene (5). 1,4-Diiodo-2,3-dihydroxybenzene (5 g, 14 mmol), K_2CO_3 (8 g, 57 mmol), and 4-(dimethylamino)pyridine (428 mg, 3.50 mmol) were placed in a 250 mL round-bottom flask capped with a rubber septum and equipped with a magnetic stir bar. The flask was then subjected to three cycles of evacuation and N_2 refill. Anhydrous dichloromethane (150 mL) was added and the reaction mixture was cooled to -78°C in an acetone/dry ice bath. Under N_2 , *tert*-butyl dicarbonate (12.2 g, 56 mmol) was dissolved in anhydrous dichloromethane (30 mL) in a separate flask and transferred by cannula to the reaction mixture at -78°C . The resulting reaction mixture was stirred while slowly warming to rt over 4 h and then left at rt overnight. In the morning, the content of the reaction was combined with a mixture of dichloromethane (50 mL), triethylamine (25 mL), and water (100 mL) and placed into a separation funnel. The organic layer was collected, dried over Na_2SO_4 , and evaporated in vacuo to give a solid that was purified by flash chromatography (10 vol % ethyl acetate in hexanes, 6×12 cm silica gel) to give a yellow product (6.1 g, 78.6 % yield). ^1H NMR (500 MHz, CDCl_3 , see Figure S9): δ 7.41 (s, 2H), 1.56 (s, 18H). ^{13}C NMR (126 MHz, CDCl_3 , see Figure S10): δ 149.4, 144.8, 137.6, 91.8, 85.0, 27.8.



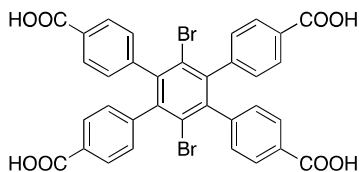
Protected 3,6-bis(pyridin-4-ylethynyl)benzene-1,2-diol (L1_a, R = Me; L1_b, R = TBS; L1_c, R = *o*NBn; L1_d, R = BOC). In a typical Sonogashira coupling, the protected 1,4-diiodo-2,3-dihydroxybenzene (2.87 mmol), copper(I) iodide (54.7 mg, 0.287 mmol), and $\text{Pd}(\text{PPh}_3)_4$ (332 mg, 0.287 mmol) were placed in a 200 mL Schlenk flask that was then subjected to three cycles of evacuation and N_2 refill. Dry tetrahydrofuran (100 mL) and diisopropylamine (50 mL) were added. Nitrogen was bubbled through the reaction mixture for 30 minutes using a long needle. Under a positive N_2 pressure, 4-ethynylpyridine hydrochloride (1 g, 7.16 mmol) was added. The flask was covered with aluminum foil (4-ethynylpyridine is light sensitive) and the reaction was allowed to proceed at rt overnight. The reaction was filtered through celite and the solvent was removed in vacuo to give a resulting solid that was purified with flash chromatography (10 vol % ethyl acetate/hexanes, gradually increasing to 50 and then to 75 vol%, 6×20 cm silica gel).

L1_a. Yield = (439 mg, 45%). ^1H NMR (500 MHz, CDCl_3 , see Figure S11): δ 8.63 (d, $J = 6.1$ Hz, 4H), 7.40 (d, $J = 6.1$ Hz, 4H), 7.24 (s, 2H), 4.04 (s, 6H). ^{13}C NMR (126 MHz, CDCl_3 , see Figure S12): δ 154.4, 149.9, 131.1, 128.2, 125.5, 118.8, 92.5, 89.4, 61.5.

L1_b. Yield = (77.5 mg, 5%). ^1H NMR (500 MHz, CDCl_3 , see Figure S13): δ 8.61 (d, $J = 6.1$ Hz, 4H), 7.36 (d, $J = 6.1$ Hz, 4H), 7.12 (s, 2H), 1.04 (s, 18H), 0.22 (s, 12H). ^{13}C NMR (126 MHz, CDCl_3 , see Figure S14): δ 150.0, 149.0, 127.0, 125.5, 118.3, 92.3, 91.9, 26.5, 18.7, -3.3.

L1_c. Yield = (736 mg, 44%). ^1H NMR (500 MHz, CDCl_3 , see Figure S15): δ 8.56 (m, 4H), 8.14 (dd, $J = 7.8, 1.4$ Hz, 2H), 8.02 (dd, $J = 8.2, 1.3$ Hz, 2H), 7.61 (dt, $J = 7.6, 1.3$ Hz, 2H), 7.45 (dt, $J = 7.8, 1.4$ Hz, 2H), 7.35 (s, 2H), 7.18 (m, 4H), 5.64 (s, 4H). ^{13}C NMR (126 MHz, CDCl_3 , see Figure S16): δ 153.2, 150.0, 146.6, 134.1, 134.1, 130.8, 129.0, 128.6, 128.5, 125.4, 125.0, 119.2, 93.3, 89.2, 72.7.

L1_d. Yield = (941 mg, 64%). ¹H NMR (500 MHz, CDCl₃, see Figure S17): δ 8.63 (d, *J* = 6.0 Hz, 4H), 7.45 (s, 2H), 7.37 (d, *J* = 6.0 Hz, 4H), 1.52 (s, 18H). ¹³C NMR (126 MHz, CDCl₃, see Figure S18): δ 150.1, 149.8, 144.76, 130.6, 130.0, 125.6, 119.4, 93.9, 87.5, 84.9, 27.7.



L2

1,4-Dibromo-2,3,5,6-tetrakis(4-carboxyphenyl)benzene (L2). **L2** was synthesized according to a literature protocol^{S3} and is a light-yellow solid (1.4 g, 57% yield). [**Safety caution**: due to pressure buildup, the synthesis of **L2** from 1,4-dibromo-2,3,5,6-tetrakis(4-methoxyphenyl)benzene in a 125 mL Parr vessel should not be carried out on a scale that is larger than 2 g of starting materials.] ¹H NMR (500 MHz, DMSO-*d*₆, see Figure S19): δ 7.78 (d, *J* = 8.0 Hz, 8H), 7.32 (d, *J* = 8.0 Hz, 8H). ¹³C NMR (126 MHz, DMSO-*d*₆, see Figure S20): δ 166.9, 144.5, 142.2, 130.1, 129.7, 128.8, 124.0.

S2. NMR spectra of ligands

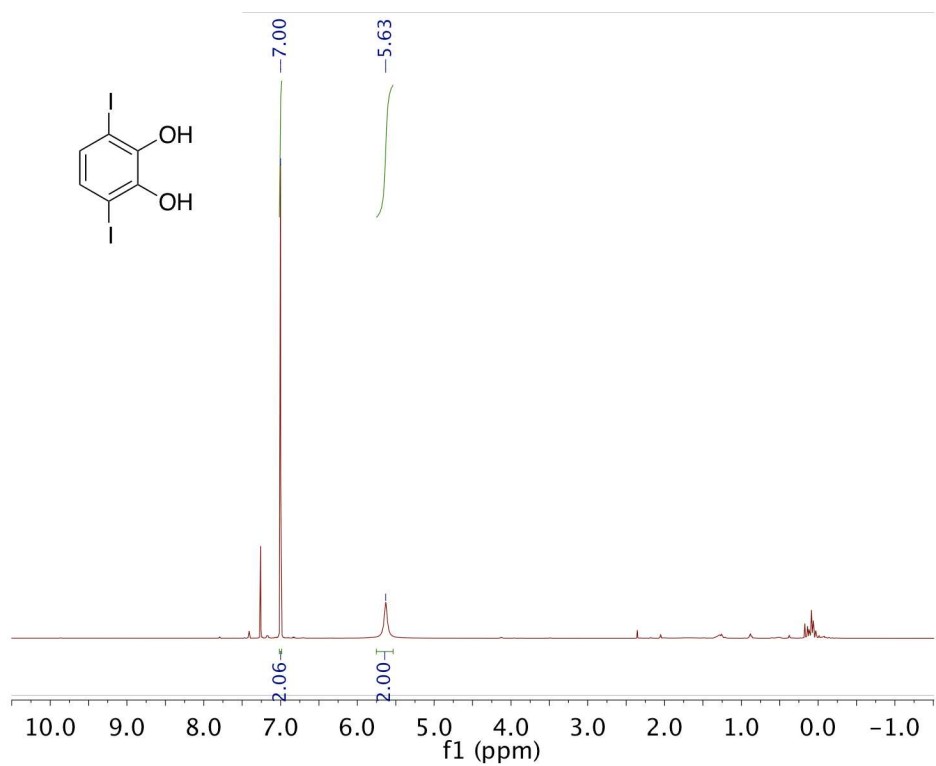


Figure S1. ^1H NMR spectrum of 1,4-diiodo-2,3-dihydroxybenzene (**1**).

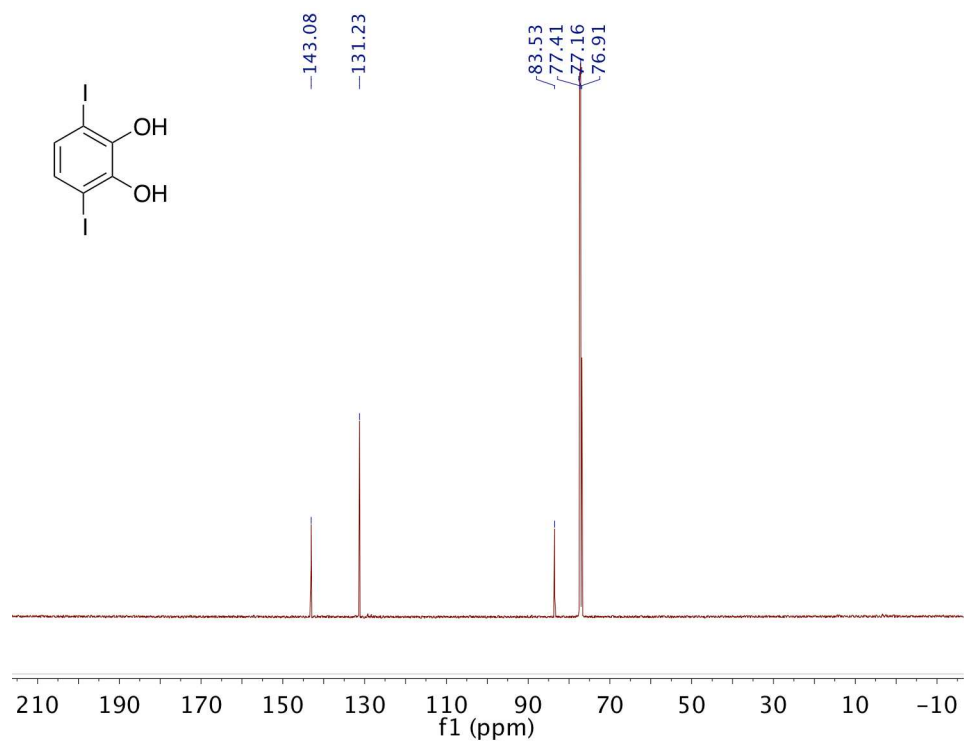


Figure S2. ^{13}C NMR spectrum of 1,4-diiodo-2,3-dihydroxybenzene (**1**).

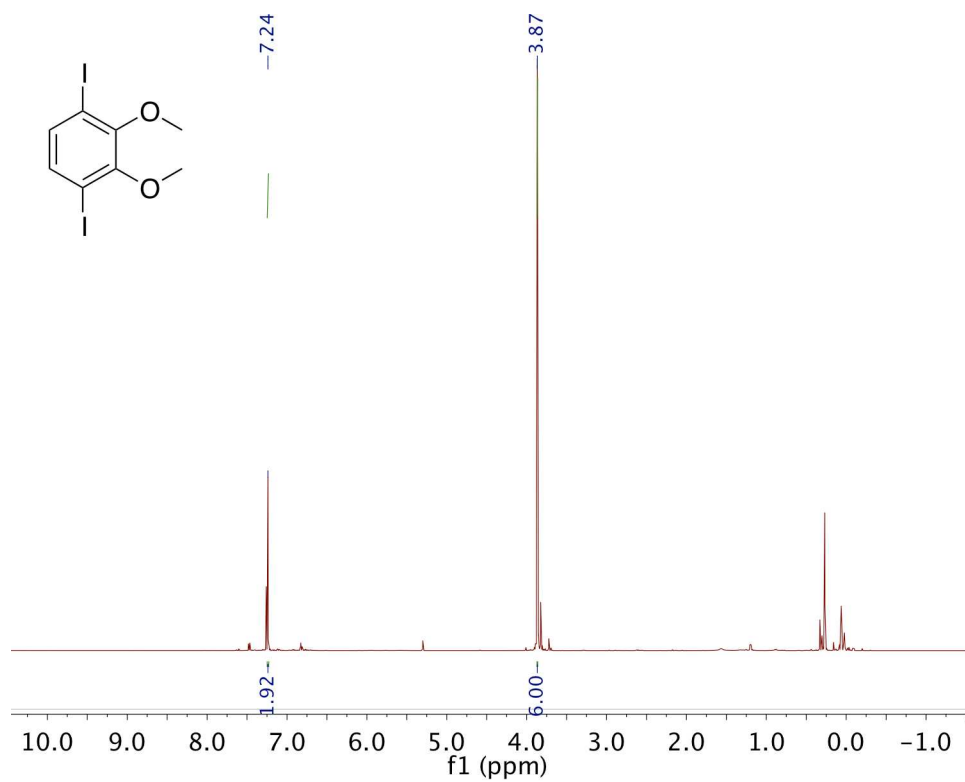


Figure S3. ^1H NMR spectrum of 1,4-diiodo-2,3-dimethoxybenzene (2).

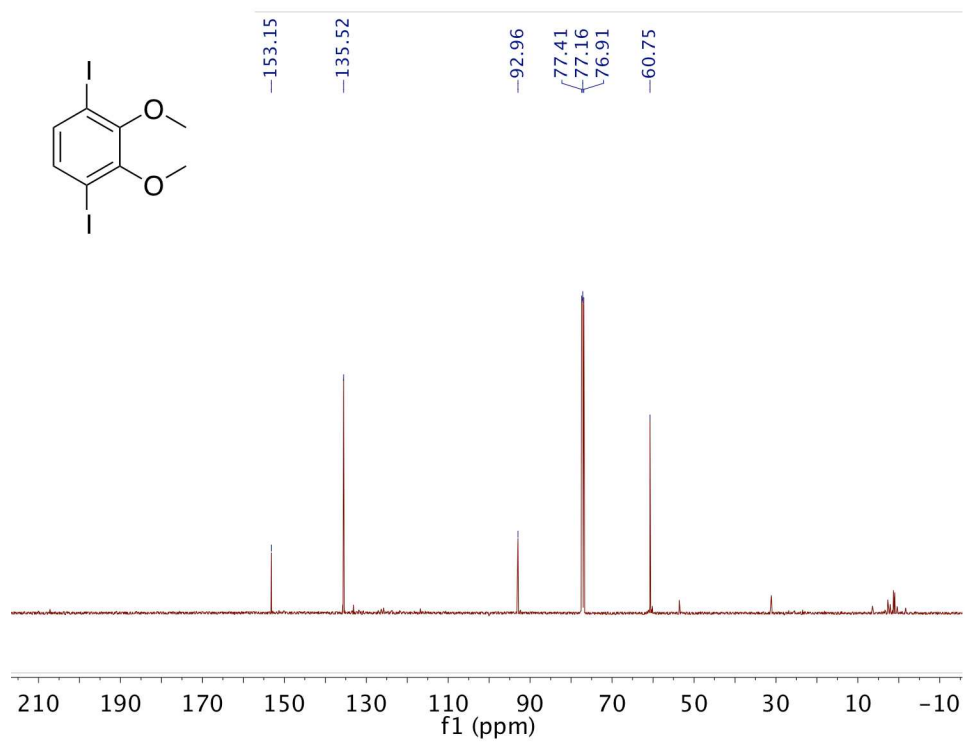


Figure S4. ^{13}C NMR spectrum of 1,4-diiodo-2,3-dimethoxybenzene (2).

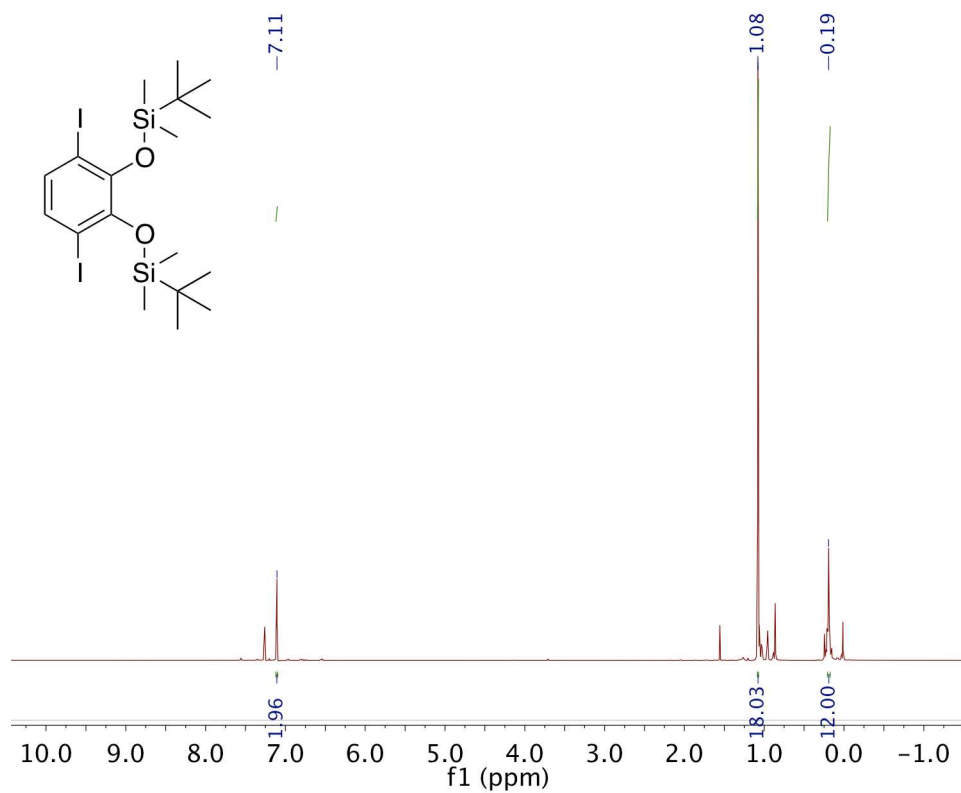


Figure S5. ¹H NMR spectrum of 2,3-bis(tert-butyldimethylsilyloxy)-1,4-diiodobenzene (**3**).

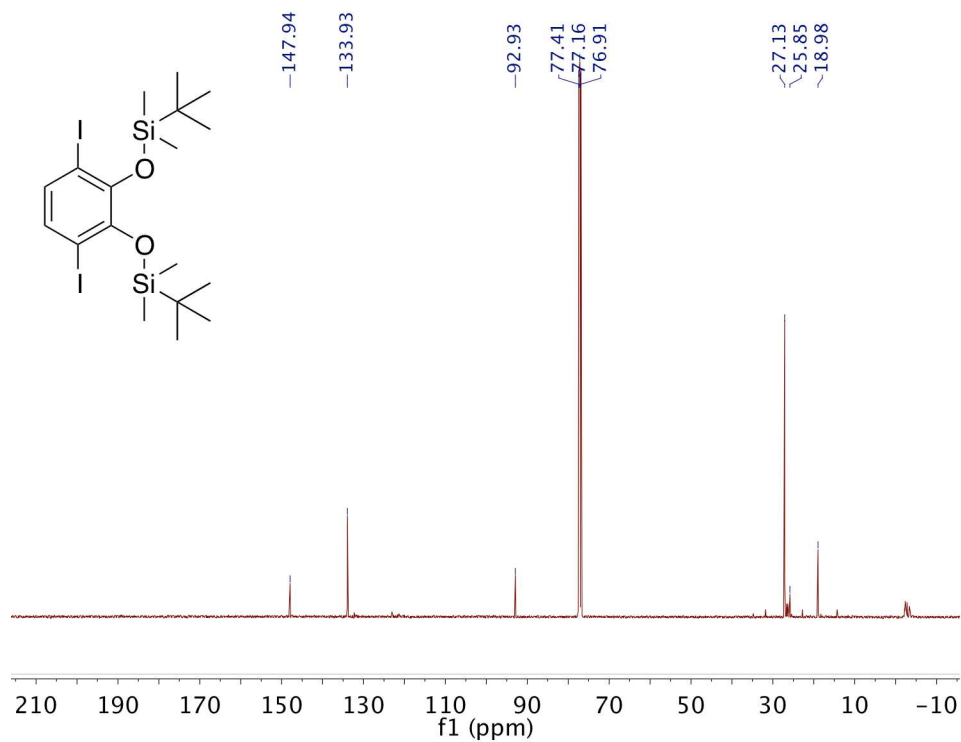


Figure S6. ¹³C NMR spectrum of 2,3-bis(tert-butyldimethylsilyloxy)-1,4-diiodobenzene (**3**).

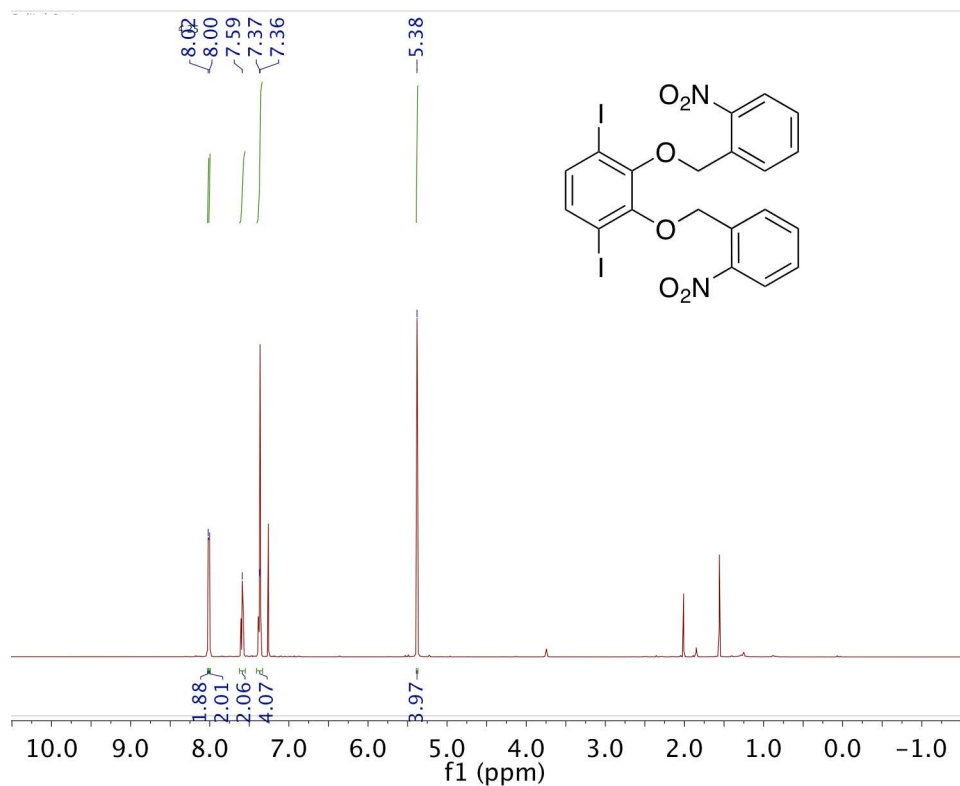


Figure S7. ^1H NMR spectrum of 1,4-diiodo-2,3-bis((2-nitrobenzyl)oxy)benzene (4).

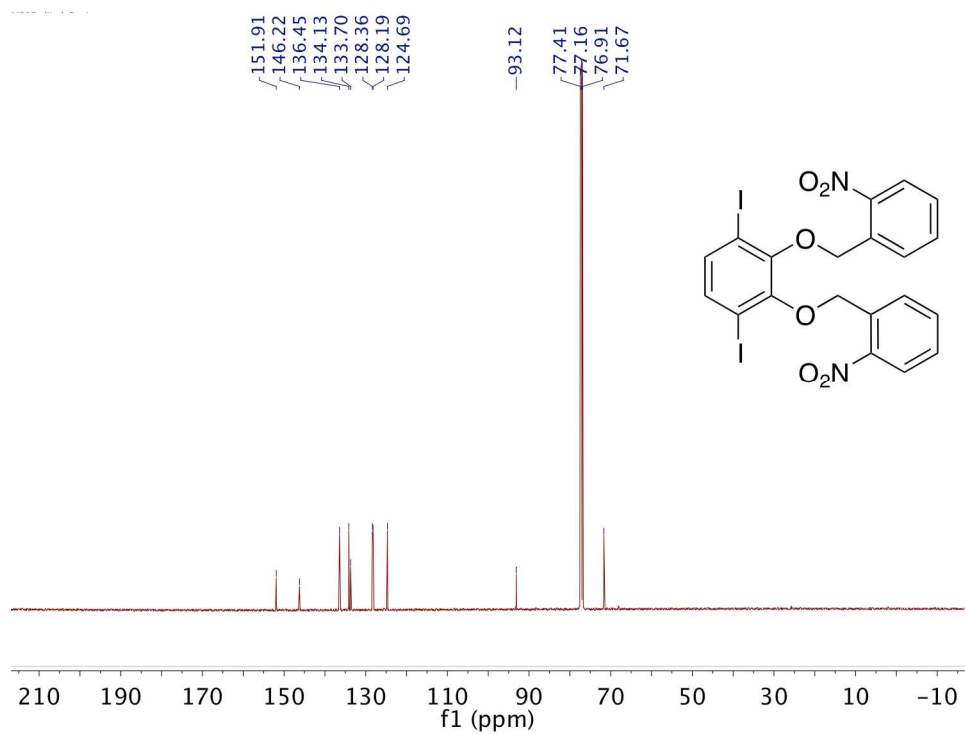


Figure S8. ^{13}C NMR spectrum of 1,4-diiodo-2,3-bis((2-nitrobenzyl)oxy)benzene (4).

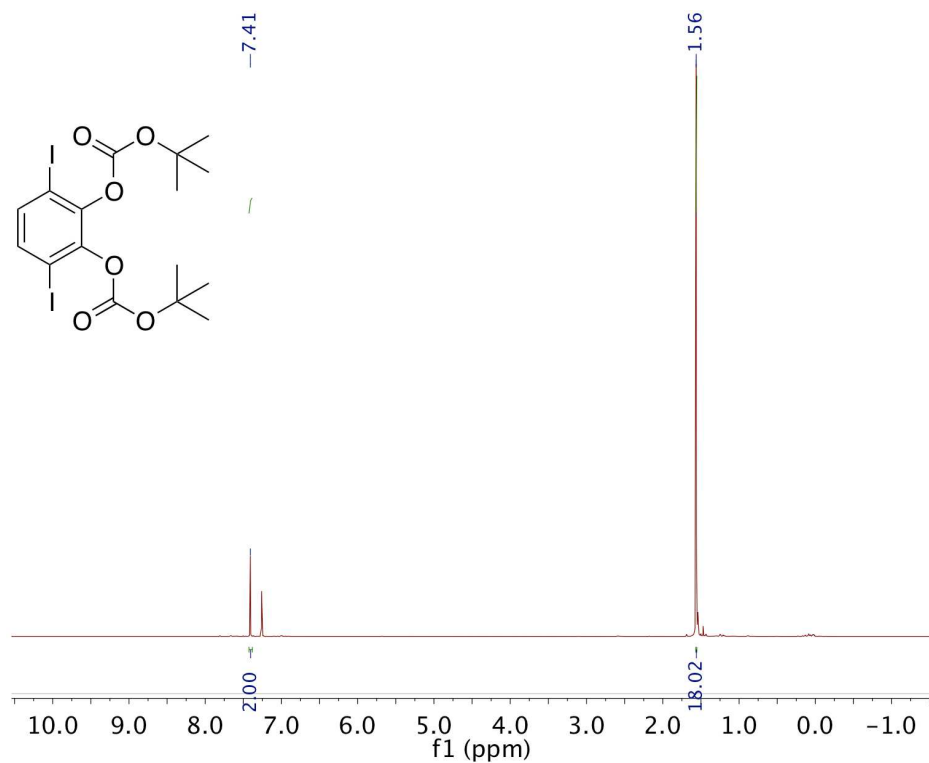


Figure S9. ^1H NMR spectrum of 1,4-diiodobenzene-2,3-bis(*tert*-butoxycarbonyloxy)benzene (**5**).

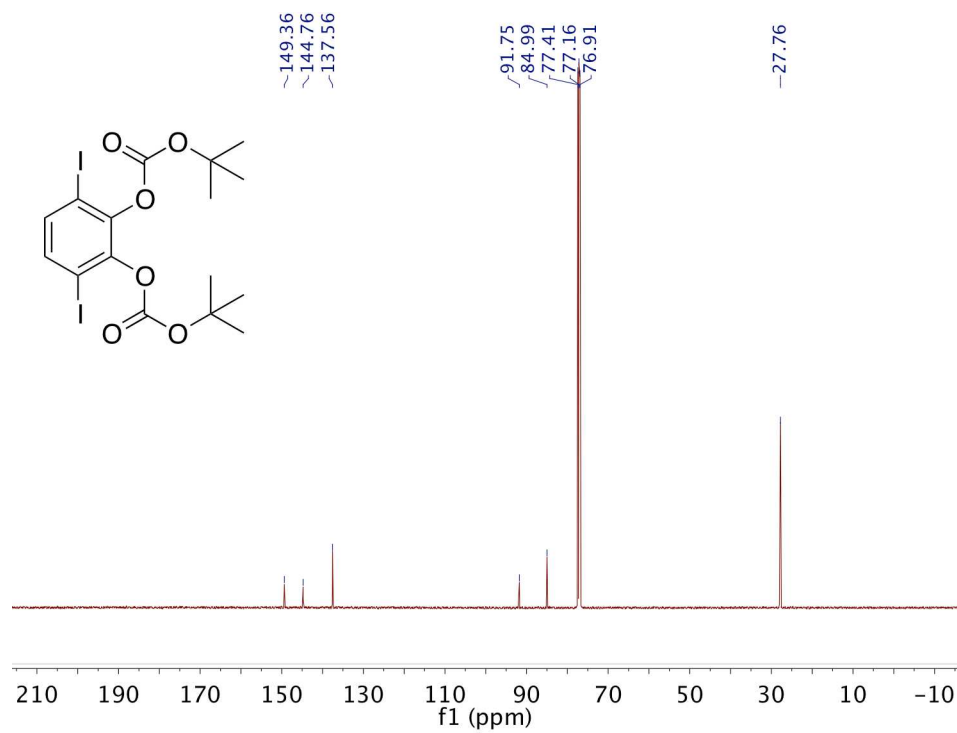


Figure S10. ^{13}C NMR spectrum of 1,4-diiodobenzene-2,3-bis(*tert*-butoxycarbonyloxy)benzene (**5**).

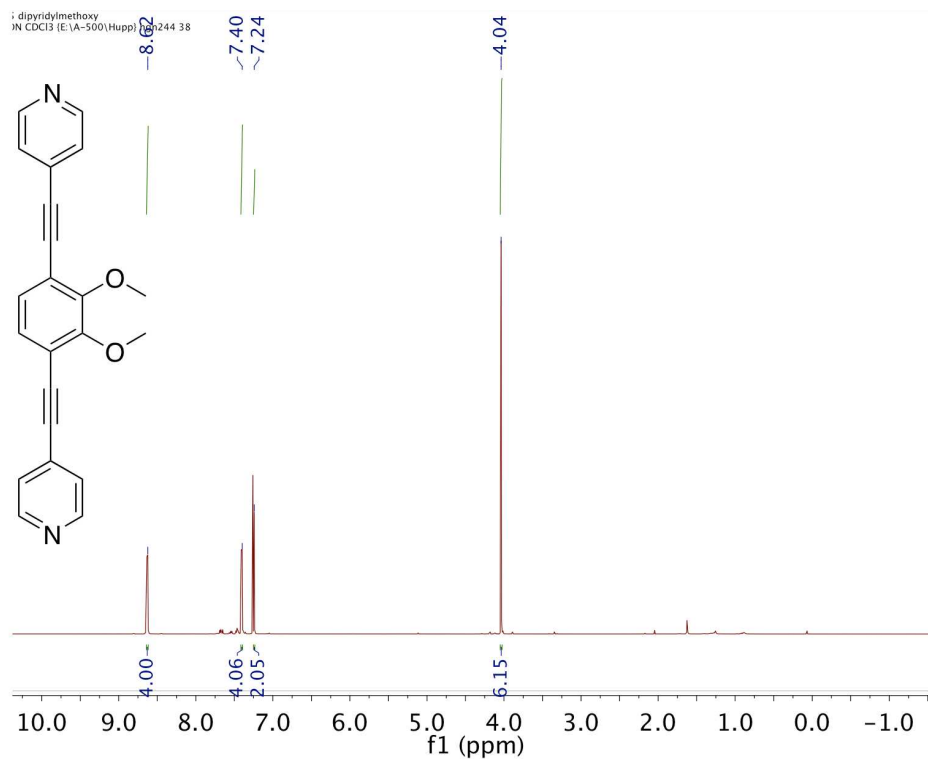


Figure S11. ¹H NMR spectrum of Me-protected 3,6-bis(pyridin-4-ylethynyl)benzene-1,2-diol (**L1_a**).

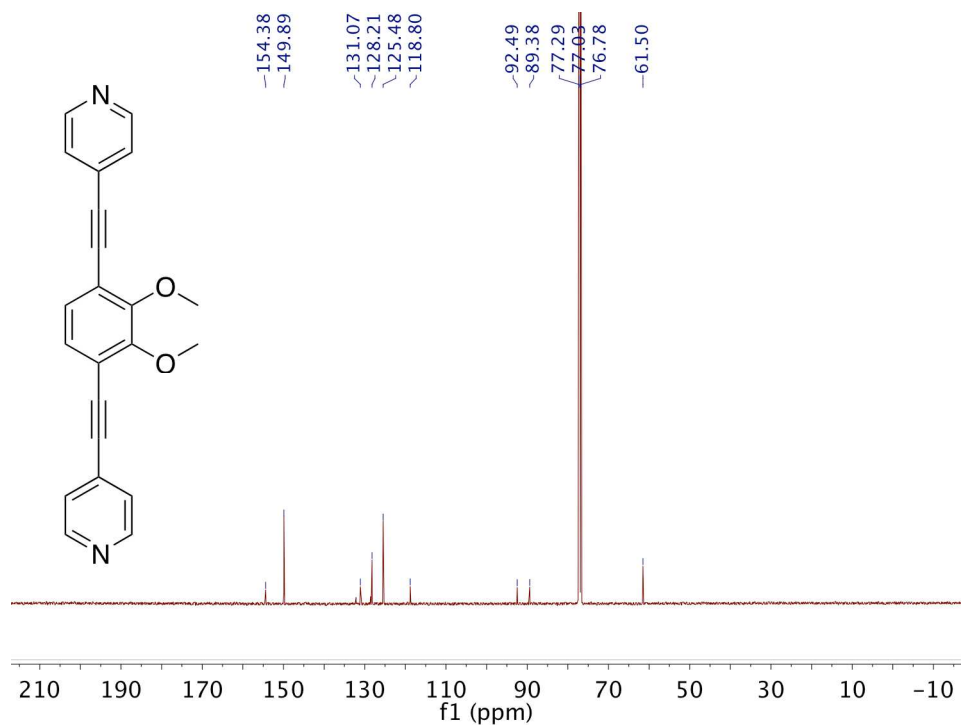


Figure S12. ¹³C NMR spectrum of Me-protected 3,6-bis(pyridin-4-ylethynyl)benzene-1,2-diol (**L1_a**).

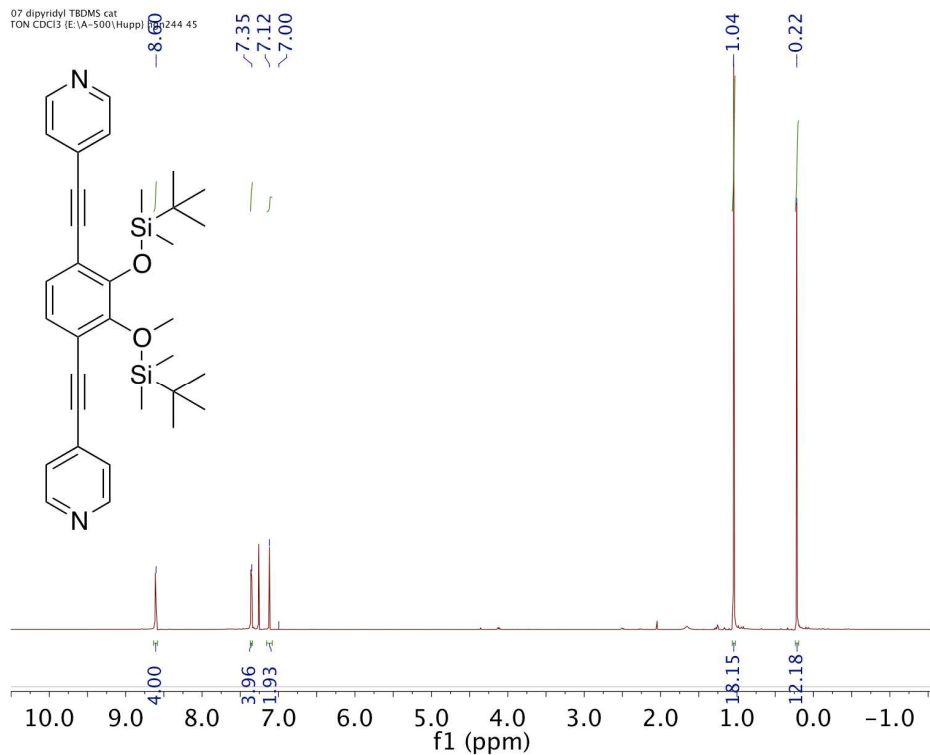


Figure S13. ¹H NMR spectrum of TBS-protected 3,6-bis(pyridin-4-ylethynyl)benzene-1,2-diol (**L1_b**).

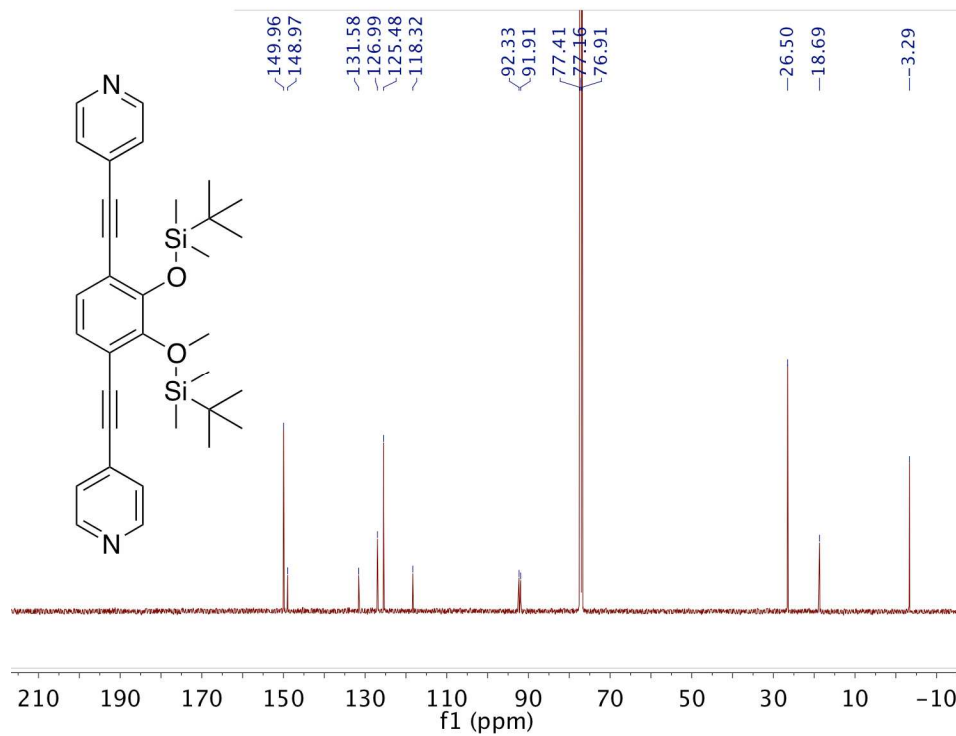


Figure S14. ¹³C NMR spectrum of TBS-protected 3,6-bis(pyridin-4-ylethynyl)benzene-1,2-diol (**L1_b**).

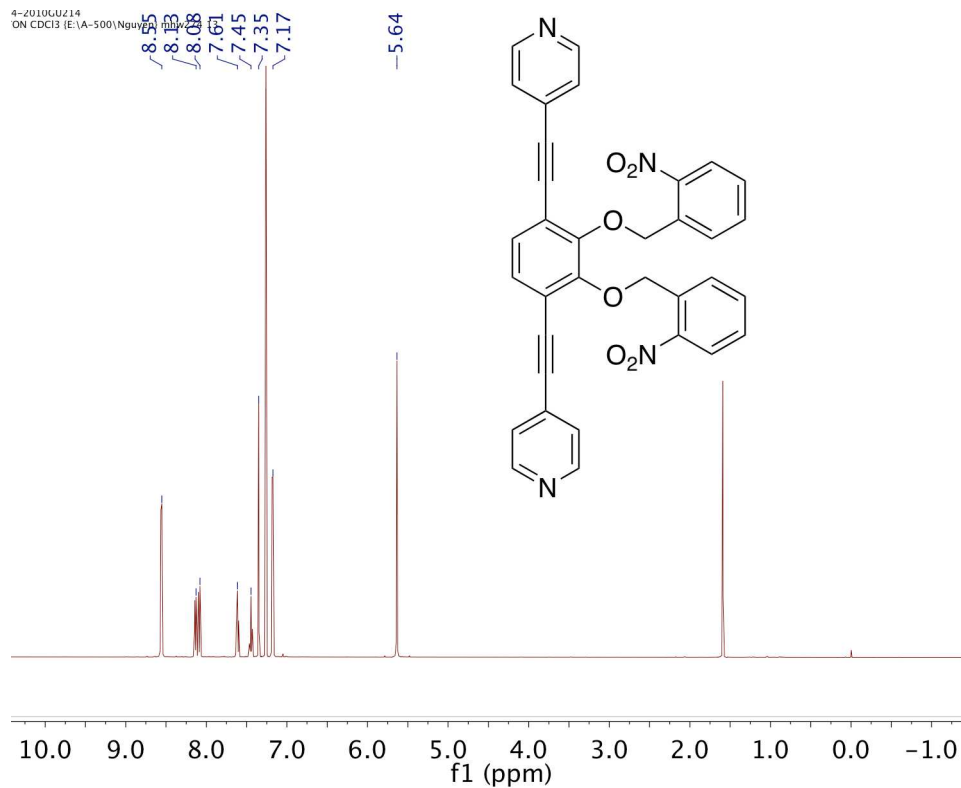


Figure S15. ¹H NMR spectrum of *o*NBn-protected 3,6-bis(pyridin-4-ylethynyl)benzene-1,2-diol (**L1c**).

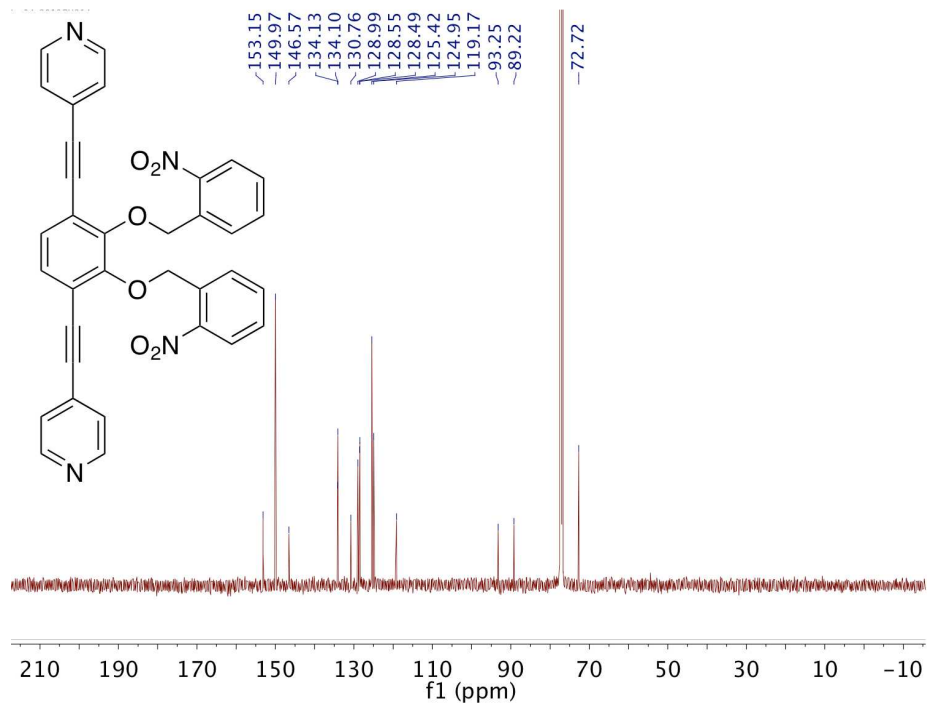


Figure S16. ¹³C NMR spectrum of *o*NBn-protected 3,6-bis(pyridin-4-ylethynyl)benzene-1,2-diol (**L1c**).

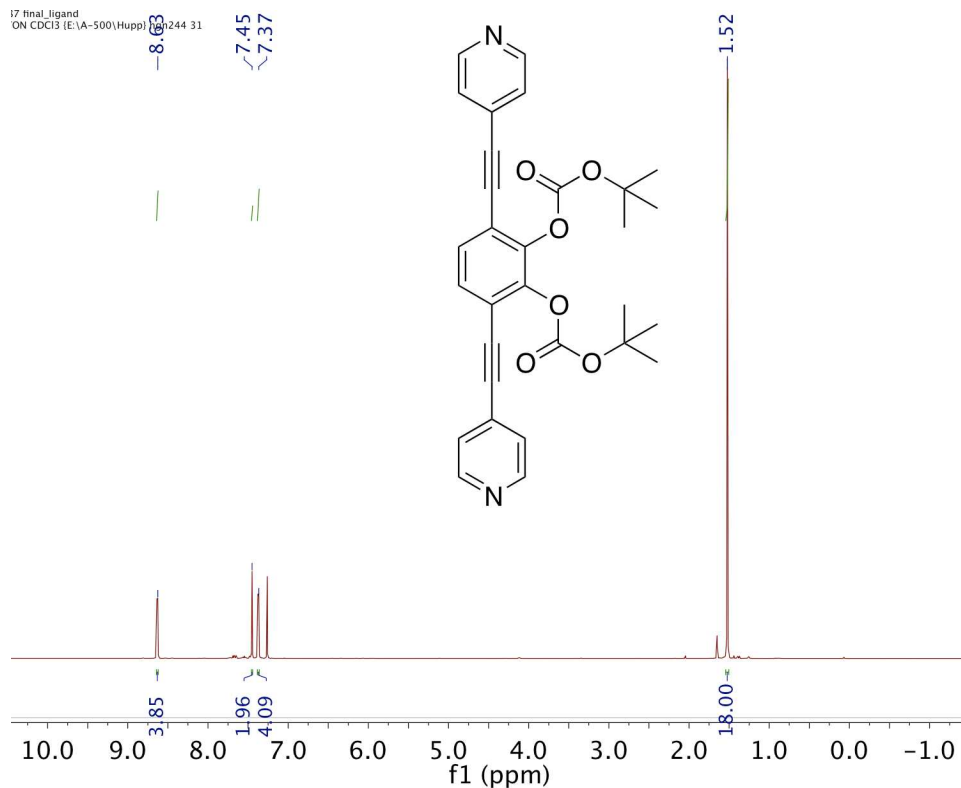


Figure S17. ¹H NMR spectrum of BOC-protected 3,6-bis(pyridin-4-ylethynyl)benzene-1,2-diol (**L1d**).

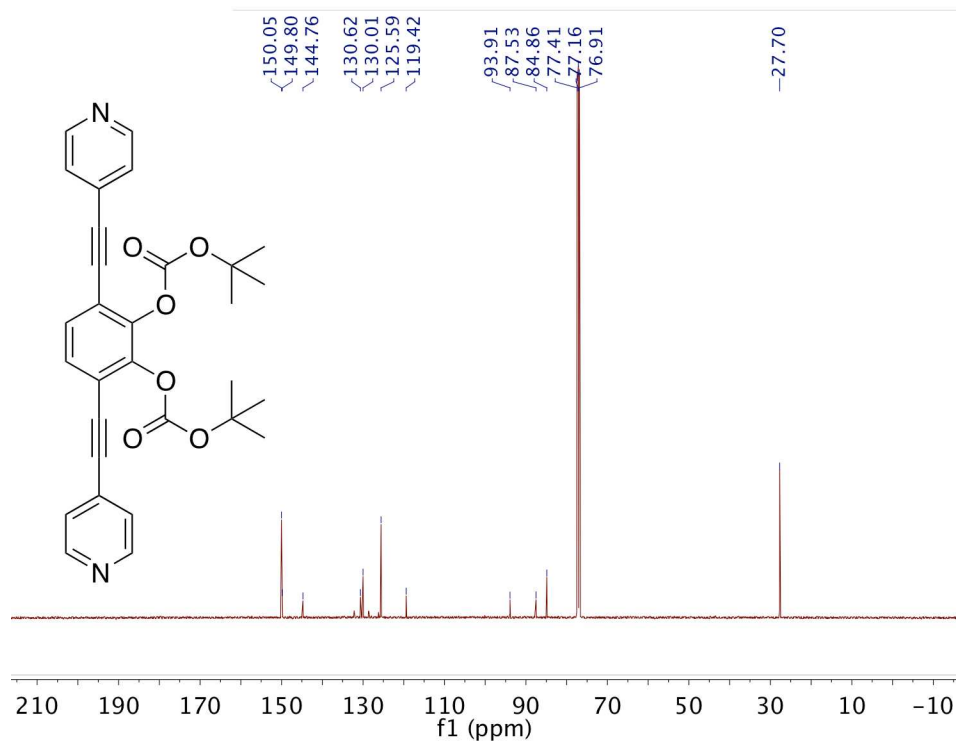


Figure S18. ¹³C NMR spectrum of BOC-protected 3,6-bis(pyridin-4-ylethynyl)benzene-1,2-diol (**L1d**).

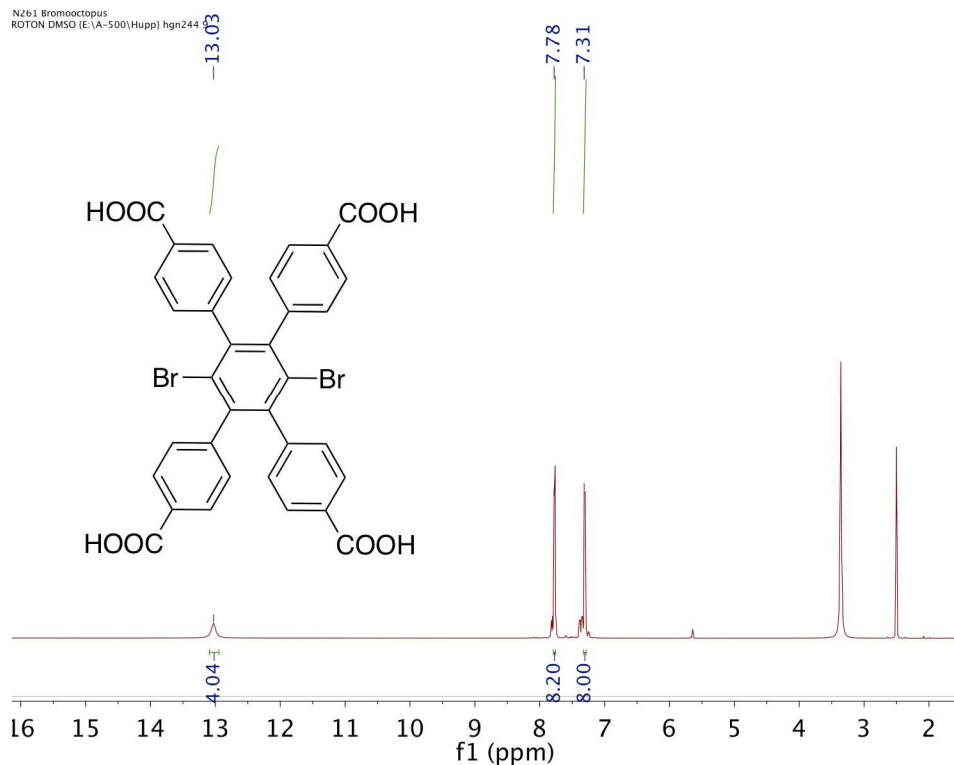


Figure S19. ^1H NMR spectrum of 1,4-dibromo-2,3,5,6-tetrakis(4-carboxyphenyl)benzene (**L2**).

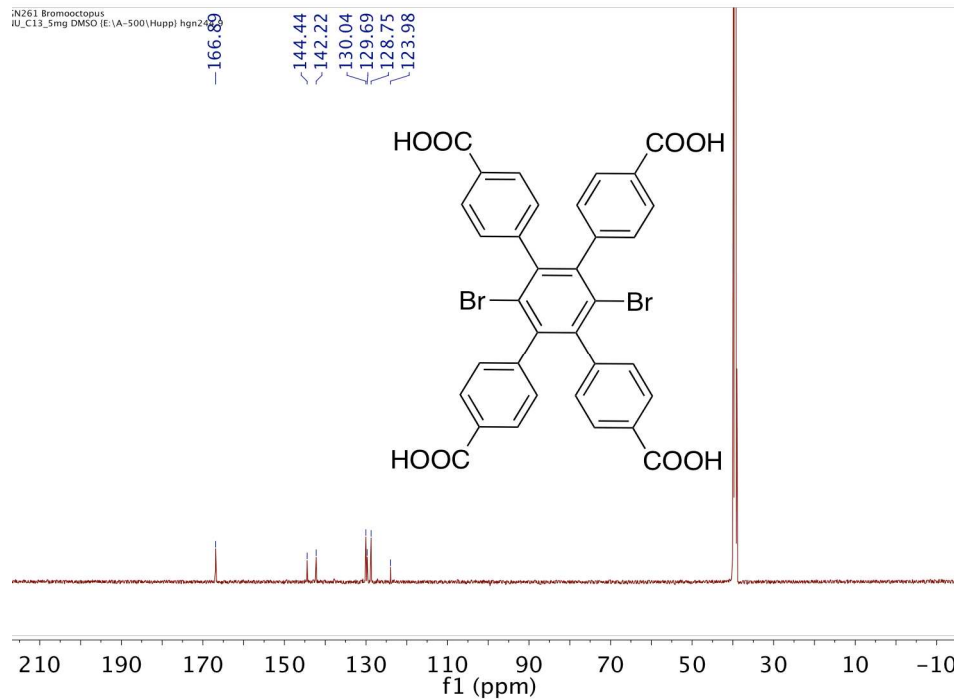


Figure S20. ^{13}C NMR spectrum of 1,4-dibromo-2,3,5,6-tetrakis(4-carboxyphenyl)benzene (**L2**).

S3. Characterization data for PG-CatBrO MOFs as well as characterization data for CatBrO MOF and V-CatBrO MOF

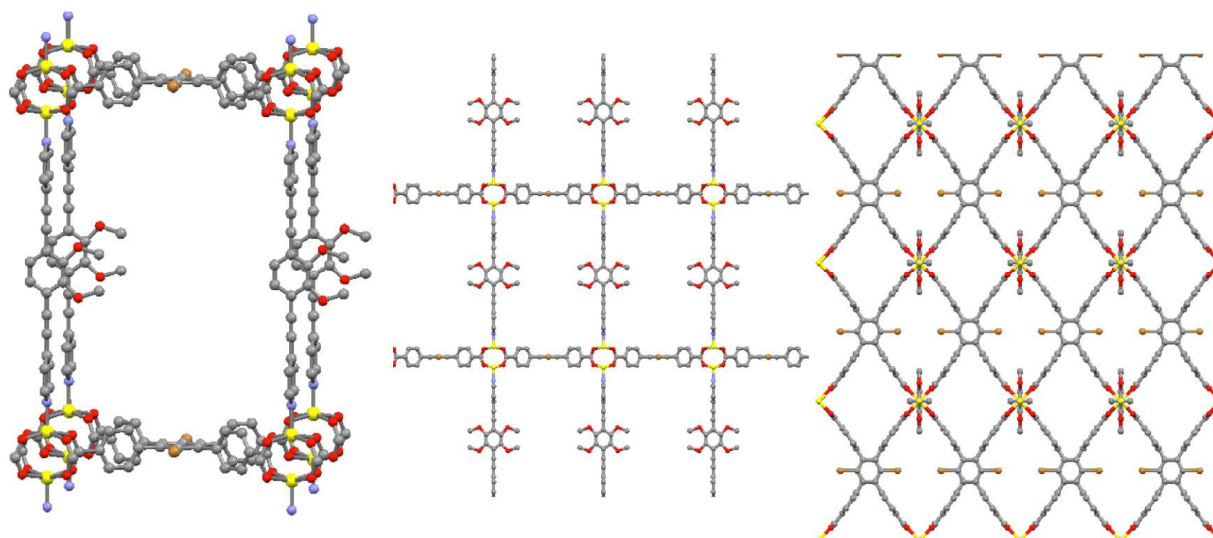


Table S1. Single-crystal X-ray diffraction data for Me-CatBrO MOF

Empirical formula	$C_{56} H_{30} Br_2 N_2 O_{10} Zn_2$	
Formula Weight	1181.38	
Temperature	225(2) K	
Wavelength	Cu K_{α} , 1.54184 Å	
Crystal system	orthorhombic	
Space group	Pmmm	
Unit cell dimension	a = 11.4439 (7) Å	$\alpha = 90^\circ$
	b = 15.7580 (9) Å	$\beta = 90^\circ$
	c = 23.466 (2) Å	$\gamma = 90^\circ$
Volume	4232.7 (5) Å ³	
Z	1	
Density (calculated)	0.464 g/cm ³	
Adsorption coefficient	1.054	
F(000)	590	
Crystal size	0.204 × 0.061 × 0.056 mm	
Theta range for data collection	3.38 to 58.57°	
Index ranges	-12 < h < 7	
	-17 < k < 16	
	-26 < l < 26	
Reflections collected	17654	
Independent reflections	3471 [R(int) = 0.101]	
Refinement method	Full-matrix least-squares on F ²	
Reflections/restraints/parameters	3472/141/114	
Goodness of fit on F ²	1.011	
Final R indices	R1 = 0.0958 wR(F2) = 0.2801 (all data)	
Largest diff. peak and hole	3.890, -0.719 e ⁻ Å ³	

Refinement Details. Refinement of F² was carried out against all reflections. The weighted R-factor wR and goodness of fit S are based on F², conventional R-factors R are based on F, with F set to zero for negative F². The threshold expression of F² > 2sigma(F²) is used only for calculating R-factors(gt), etc. and is not relevant to the choice of reflections for refinement. R-factors based on F² are statistically about twice as large as those based on F, and R-factors based on all data will be even larger.

Restraints based on literature values from a search of similar fragments in the CSD were applied to the C11-C12 triple bond and the C-O and Me-C(Ph) distances, (esd's = 0.001). Similarity restraints were applied to the C10-C11

and C12-C13 distances, as well as all ortho C-C distances in the pyridine and phenyl rings of that strut. Global rigid bond (DELU) and similarity (SIMU) restraints were applied to keep displacement parameters reasonable.

Solvent Treatment Details. A solvent-masking procedure, as implemented in Olex2, was used to remove the electronic contribution of solvent molecules from the refinement. Only the atoms used in the refinement model are reported in the formula here. Total solvent-accessible volume/cell = 3305.0 Å³ [78.1%]. Total electron count/cell = 1045.4.

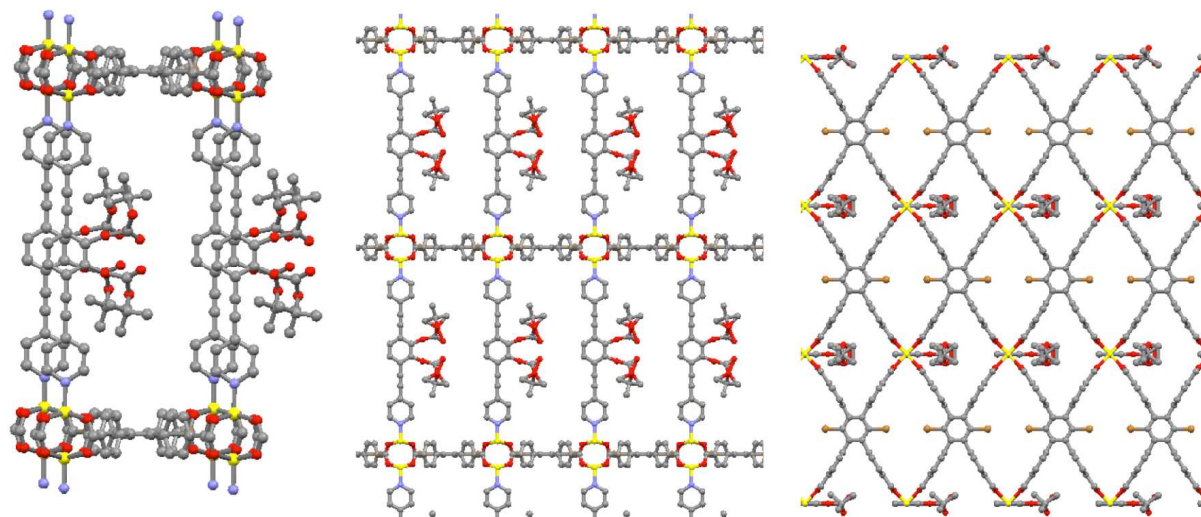


Table S2. Single-crystal X-Ray diffraction data for **BOC-CatBrO MOF**.

Empirical formula	C ₆₁ H ₃₃ Br ₂ N ₂ O ₁₄ Zn ₂	
Formula Weight	1308.45	
Temperature	100(2) K	
Wavelength	Cu K α , 1.54184 Å	
Crystal system	orthorhombic	
Space group	Pmmm	
Unit cell dimension	a = 10.9619 (11) Å	$\alpha = 90^\circ$
	b = 16.0098 (14) Å	$\beta = 90^\circ$
	c = 23.383 (4) Å	$\gamma = 90^\circ$
Volume	4103.7 (9) Å ³	
Z	1	
Density (calculated)	0.529 g/cm ³	
Adsorption coefficient	1.128	
F(000)	655	
Crystal size	0.282 × 0.126 × 0.06 mm	
Theta range for data collection	4.03 to 58.15°	
Index ranges	-10 < h < 9	
	-15 < k < 15	
	-23 < l < 23	
Reflections collected	12093	
Independent reflections	2382 [R(int) = 0.0590]	
Refinement method	Full-matrix least-squares on F ²	
Reflections/restraints/parameters	2382/220/155	
Goodness of fit on F ²	1.173	
Final R indices	R1 = 0.1208 wR(F2) = 0.3460 (all data)	
Largest diff. peak and hole	2.486, -0.785 e ⁻ Å ³	

Refinement Details. Refinement of F^2 was carried out against all reflections. The weighted R-factor wR and goodness of fit S are based on F^2 , conventional R-factors R are based on F , with F set to zero for negative F^2 . The threshold expression of $F^2 > 2\sigma(F^2)$ is used only for calculating R-factors(gt), etc. and is not relevant to the choice of reflections for refinement. R-factors based on F^2 are statistically about twice as large as those based on F , and R-factors based on all data will be even larger.

Chemically equivalent C-O, C-C, C-N, N-O, and O-O distances were refined with similarity restraints (SADI). FLAT restraints were applied to phenyl rings containing C42a, C49 and C49a. Global rigid bond (DELU, esd 0.01) and similarity (SIMU, esd 0.04, 0.08, 1.7 Ang) restraints were applied to keep displacement parameters reasonable. A full list of restraints is given in the IUCR-refine-details section of the CIF file.

Solvent Treatment Details. A solvent-masking procedure, as implemented in Olex2, was used to remove the electronic contribution of solvent molecules from the refinement. Only the atoms used in the refinement model are reported in the formula here. Total solvent-accessible volume/cell = 2897.3 Å³ [22.1%]. Total electron count/cell = 714.6.

Table S3. Single-crystal X-Ray diffraction data for *o*NBn-CatBrO MOF.

Empirical formula	C ₆₈ H ₃₈ Br ₂ N ₄ O ₁₄ Zn ₂	
Formula Weight	1425.62	
Temperature	100(2) K	
Wavelength	Cu K α , 1.54184 Å	
Crystal system	orthorhombic	
Space group	Pmmm	
Unit cell dimension	a = 11.0768 Å	$\alpha = 90^\circ$
	b = 15.9740 Å	$\beta = 90^\circ$
	c = 23.4082 Å	$\gamma = 90^\circ$

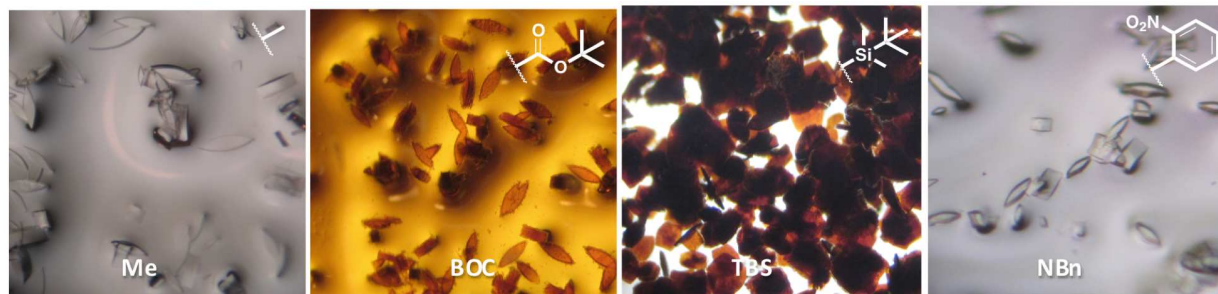


Figure S21. Photographic images of Me-CatBrO MOF (left), BOC-CatBrO MOF (middle left), TBS-CatBrO MOF (middle-right), and *o*NBn-CatBrO MOF (right) viewed under a light microscope.

EA data for BOC-CatBrO MOF. %C = 49.79, %H = 2.57, %N = 2.70; theoretical: %C = 56.70, %H = 3.27, %N = 2.07,

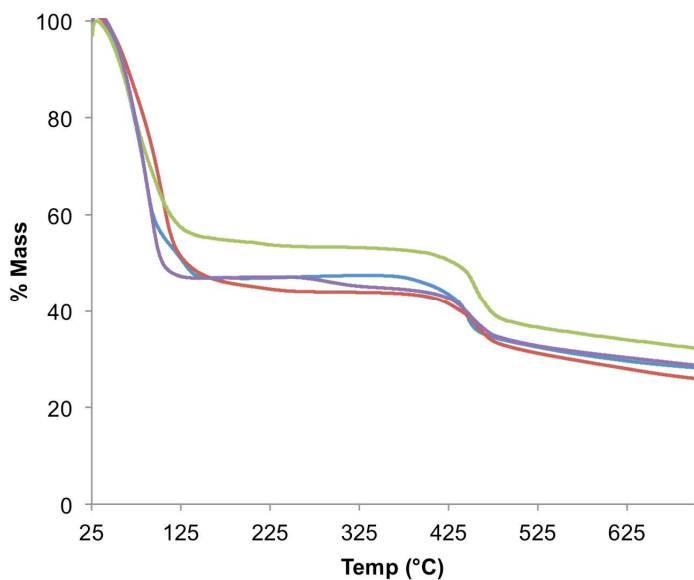


Figure S22. TGA profiles of **Me-CatBrO-MOF** (blue), **BOCCatBrO-MOF** (red), **TBS-CatBrO MOF** (green), and **oNBn-CatBrO MOF** (purple). Solvent makes up about 45-55% of the mass and MOF decomposition occurs around 450 °C.

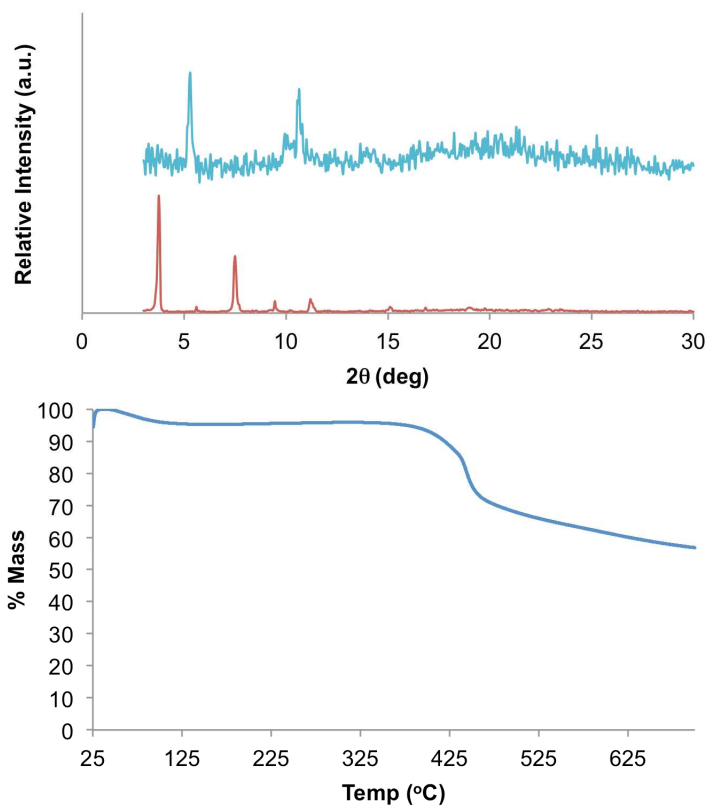


Figure S23. Top: Simulated (red) and experimental (blue) PXRD patterns of thermally activated **PG-CatBrO MOF** after resolution. Bottom: TGA profile of activated **PG-CatBrO MOF** after resolution.

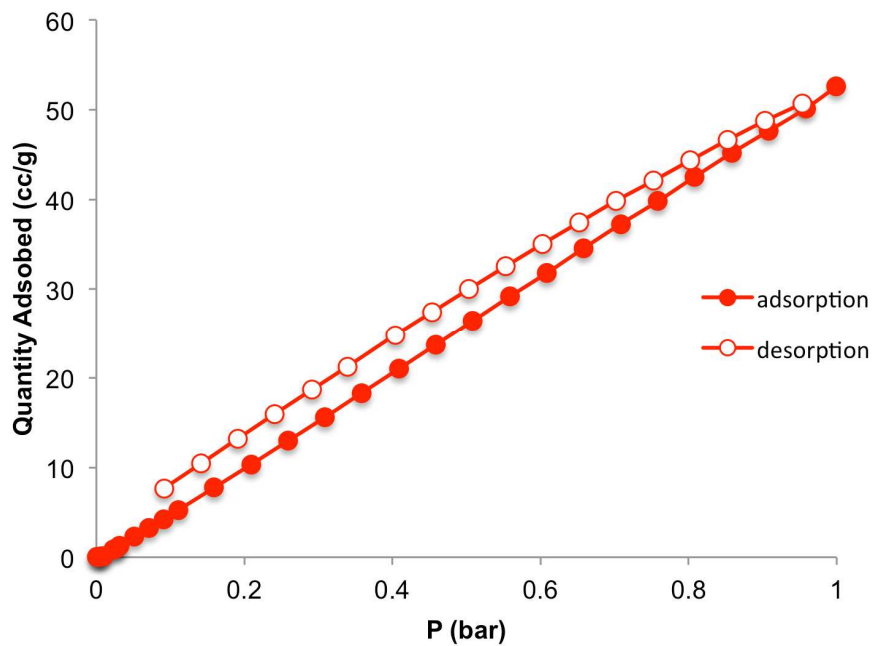


Figure S24. CO₂ isotherms of Me-CatBrO MOF at 273K.

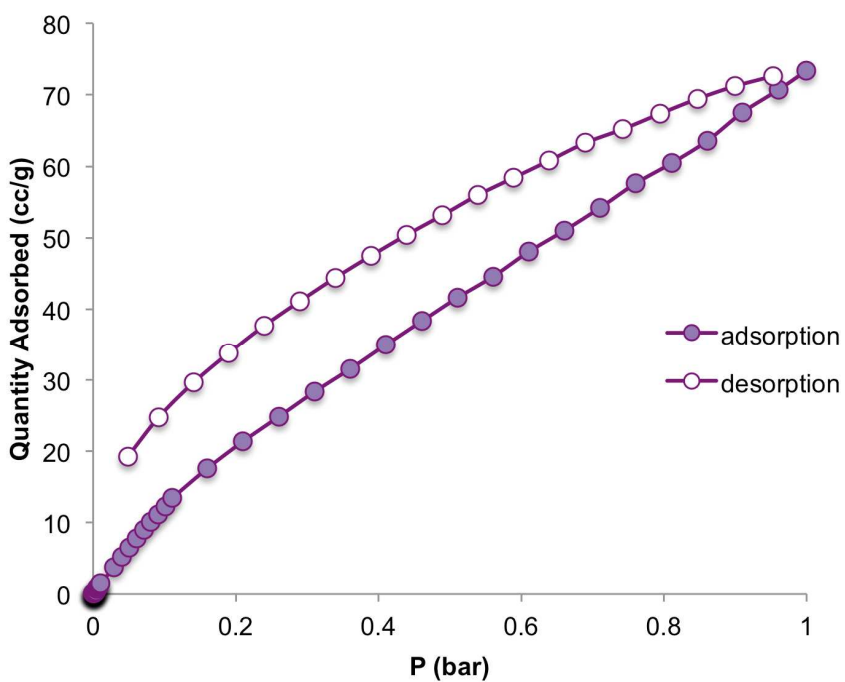


Figure S25. CO₂ isotherms of TBS-CatBrO MOF at 273K.

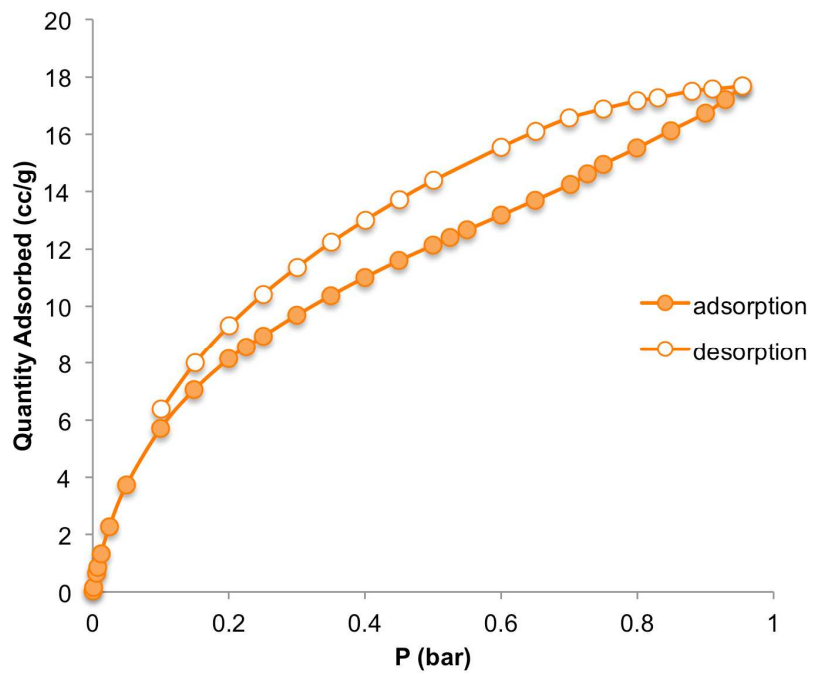


Figure S26. CO₂ isotherms of *o*NBn-CatBrO MOF at 273K.

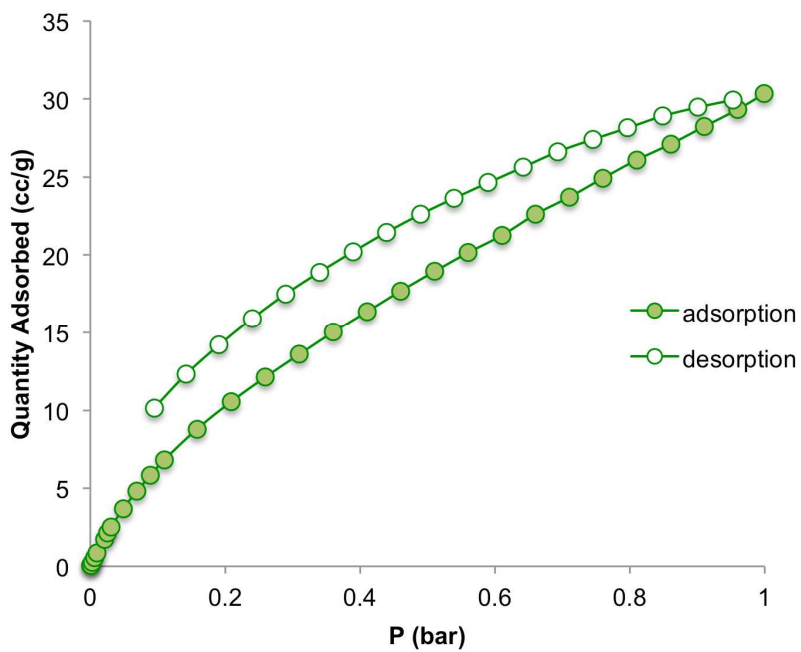


Figure S27. CO₂ isotherms of BOC-CatBrO MOF at 273K.

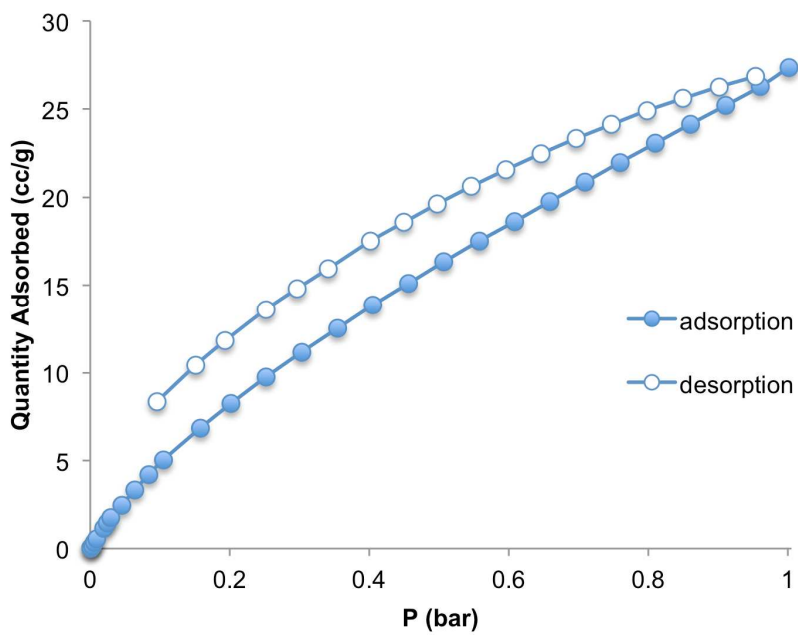


Figure S28. CO₂ isotherms of thermally deprotected CatBrO-MOF at 273K.

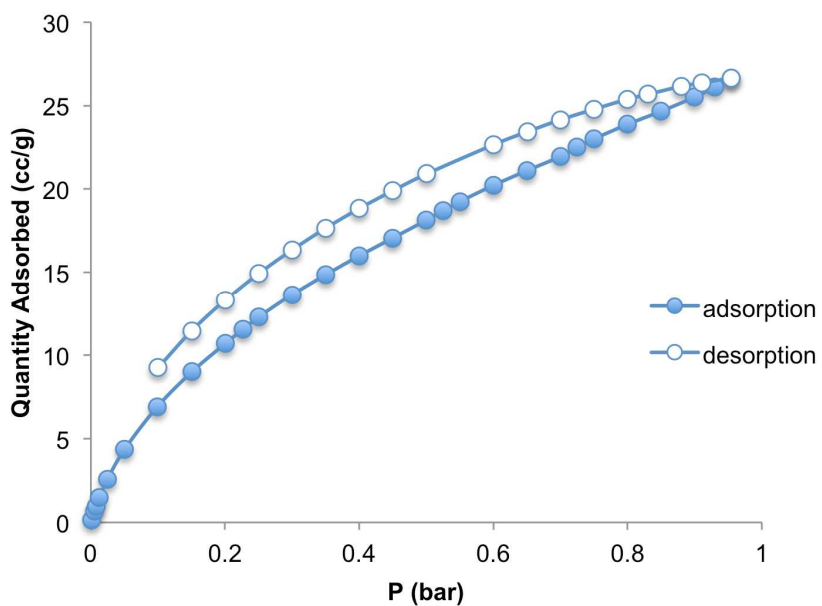


Figure S29. CO₂ isotherms of UV-deprotected CatBrO MOF at 273K.

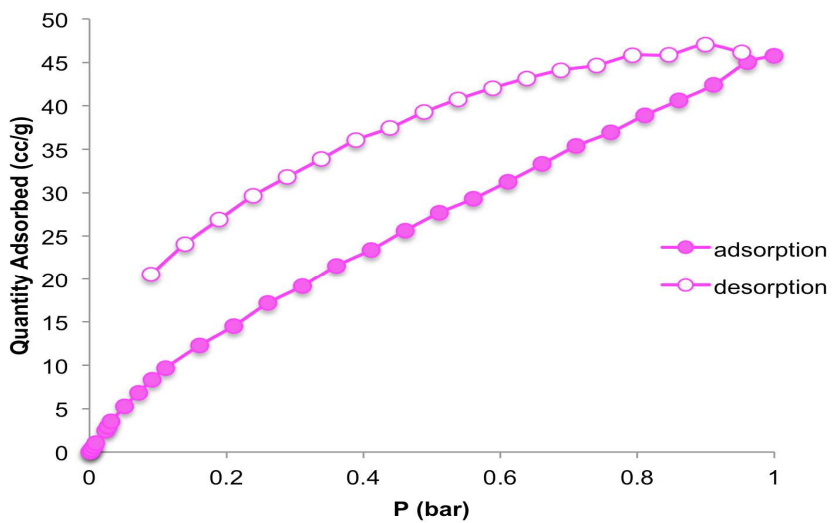


Figure S30. CO₂ isotherms of V-CatBrO MOF at 273K.

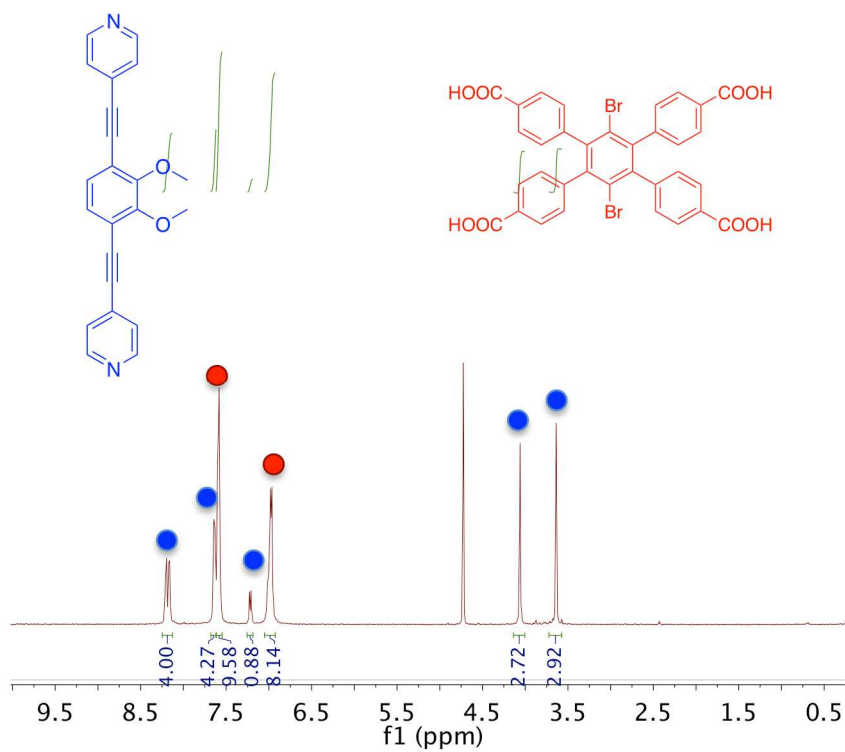


Figure S31. The ¹H NMR spectrum of Me-CatBrO MOF after digestion in D₂SO₄, showing the expected 1:1 ratio of L1_a (blue ligand) and L2 (red ligand).

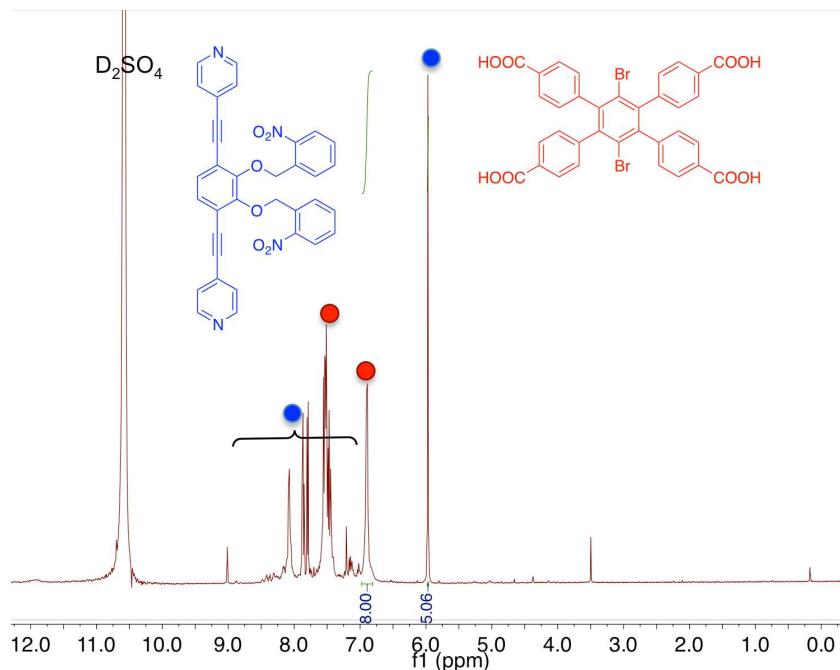


Figure S32. The ¹H NMR spectrum of *o*NBn-CatBrO MOF after digestion in D₂SO₄, showing an ~ 1.3:1 ratio of L_{1c} (blue ligand) and L₂ (red ligand). The *o*NBn-protected dipyriddy ligand (L_{1c}) in MOF was degraded in conc. D₂SO₄, giving no identifiable peaks in the aromatic region.

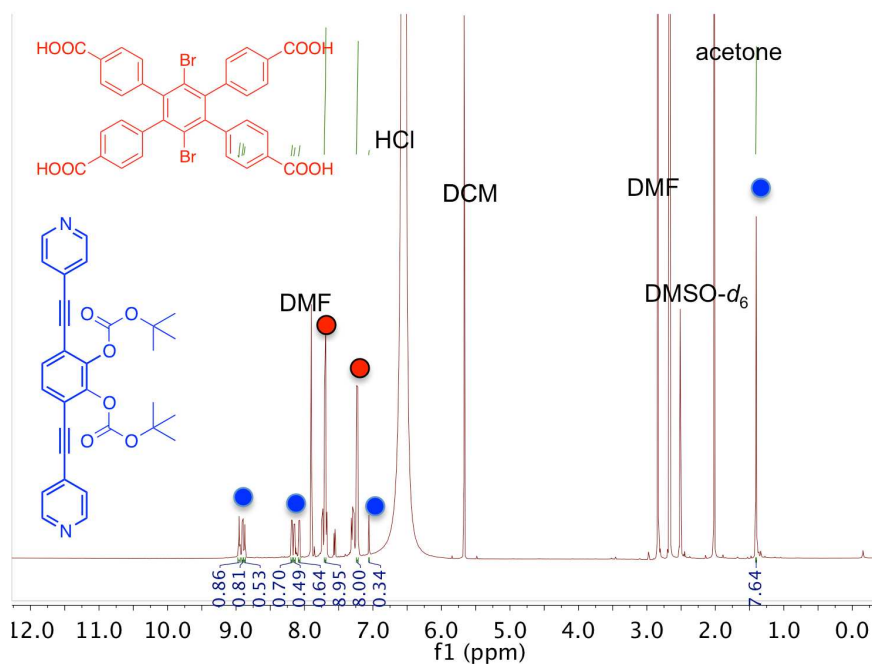


Figure S33. The ¹H NMR spectrum of BOC-CatBrO MOF after digestion in a 1:9 v/v mixture of conc. HCl:DMSO-*d*₆ showing an ~ 0.6:1 ratio of L_{1d} (blue ligand) and L₂ (red ligand). The low ratio of the *tert*-butyl protons to aromatic protons of L_{1d} suggested that up to ~1/4 of the BOC groups were missing.

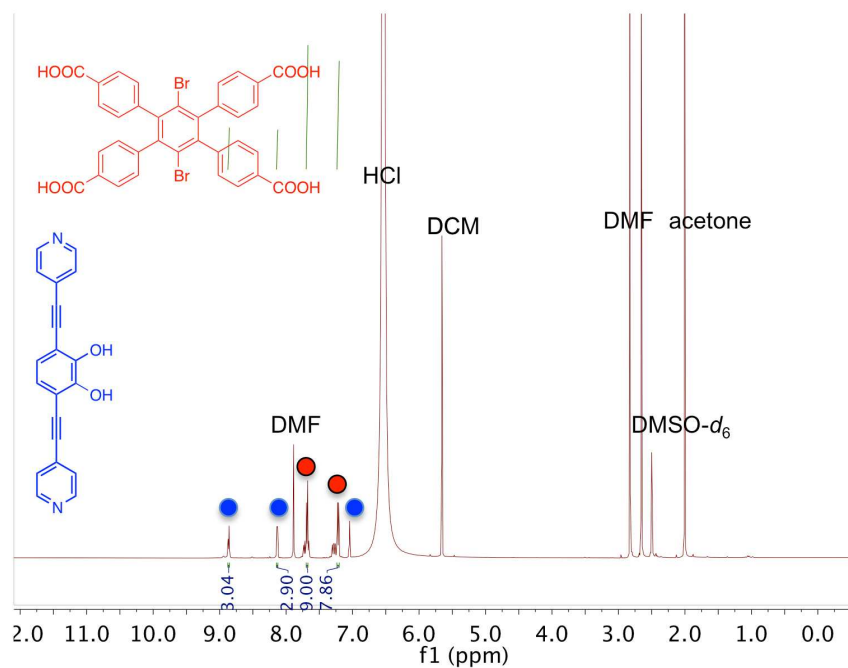


Figure S34. The ^1H NMR spectrum of **CatBrO MOF** after digestion in a 1:9 v/v mixture of conc. HCl:DMSO- d_6 showing an $\sim 0.7:1$ ratio of **L1_d** (blue ligand) and **L2** (red ligand).

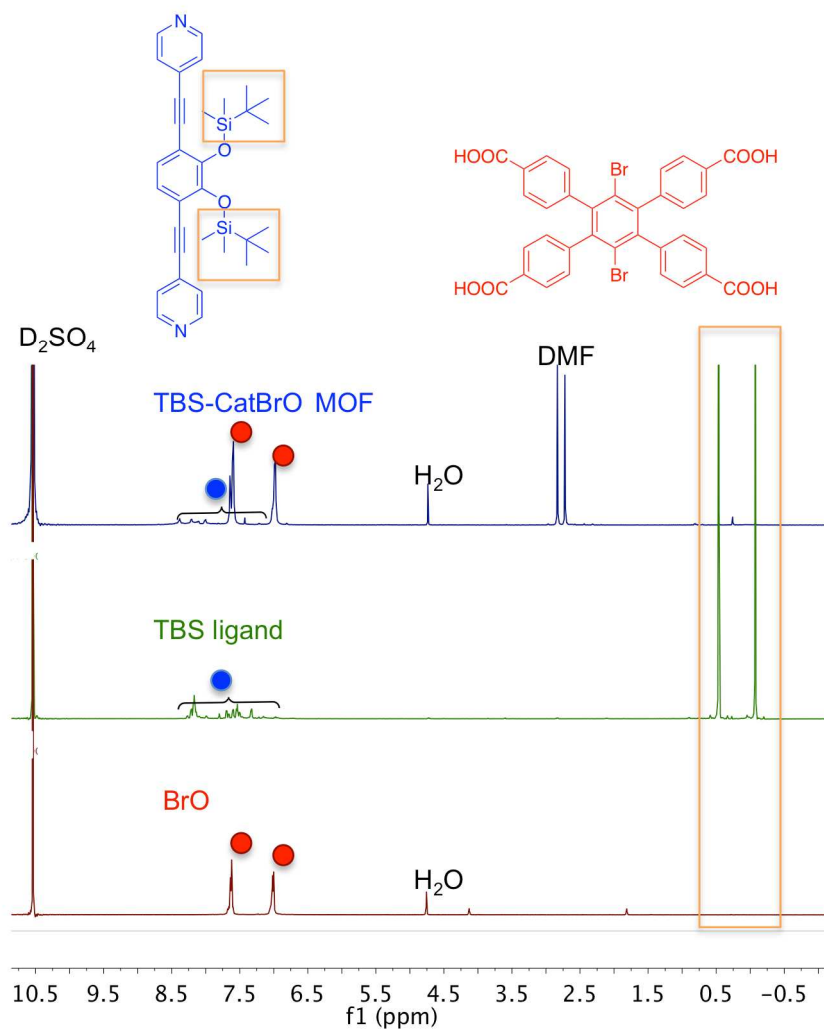


Figure S35. ¹H NMR spectra of **L2**, **L1_b**, and **TBS-CatBrO MOF** after digestion in D₂SO₄ (bottom to top), illustrating the expected absence of the TBS group in **TBS-CatBrO MOF** after digestion. The TBS-protected dipyriddy ligand (**L1_b**) was degraded in conc. D₂SO₄, giving no identifiable peaks in the aromatic region.

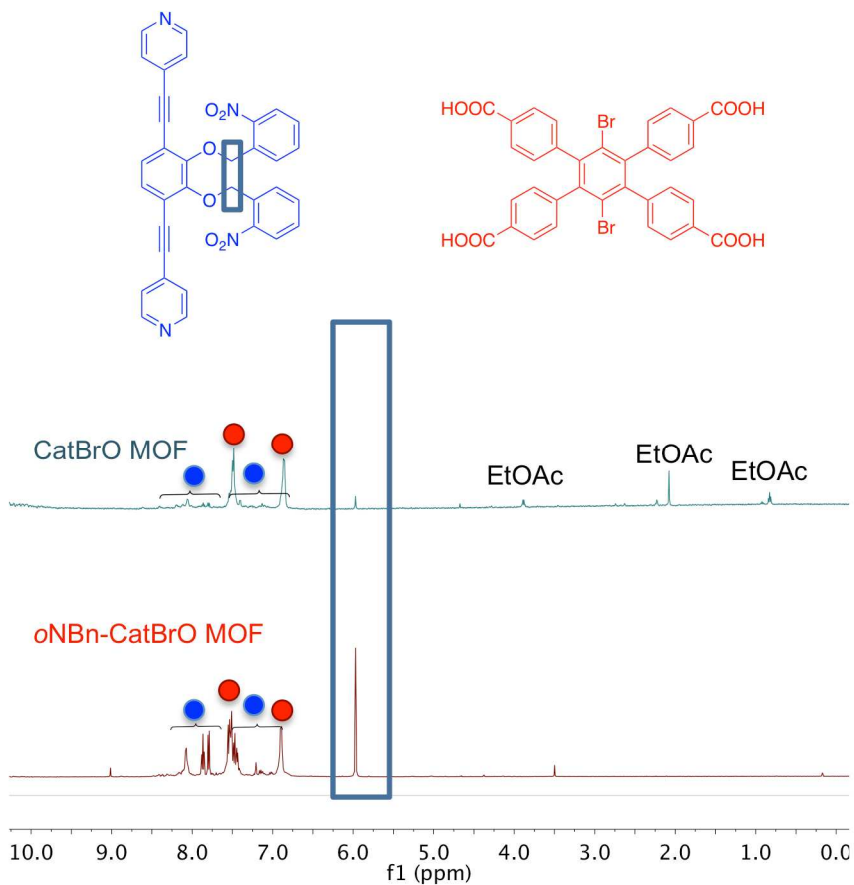


Figure S36. ^1H NMR spectra of *o*NBn-CatBrO-MOF before (bottom) and after UV irradiation (top), showing the diminishing benzylic protons peak and indicating that CatBrO-MOF is produced. The *o*NBn-protected dipyriddy ligand (**L1**) in the MOF was degraded in conc. D_2SO_4 , giving no identifiable peaks in the aromatic region.

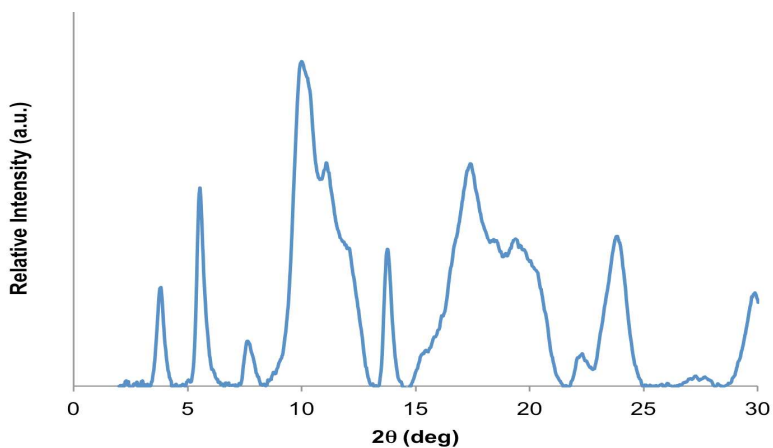


Figure S37. PXRD pattern (obtained via capillary methods) of *o*NBn-CatBrO MOF after UV irradiation and stirring, showing partial loss in crystallinity.

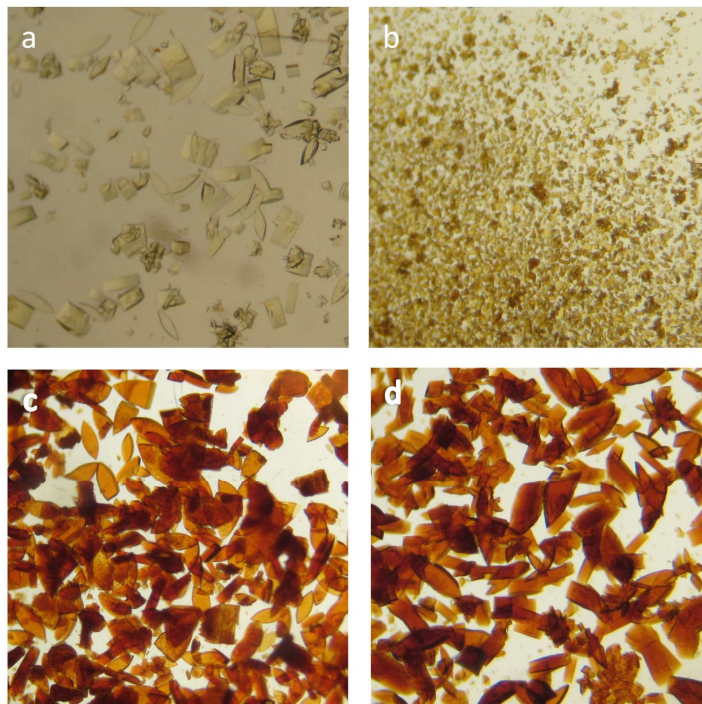


Figure S38. (a-b) Photographic images (taken under light microscope) of *o*NBn-CatBrO MOF: (a) before and (b) after photodeprotection, showing fragmentation of crystals in (b). (c-d) Photographic images (taken under light microscope) of BOC-CatBrO MOF (c) and thermally deprotected CatBrO MOF (d).

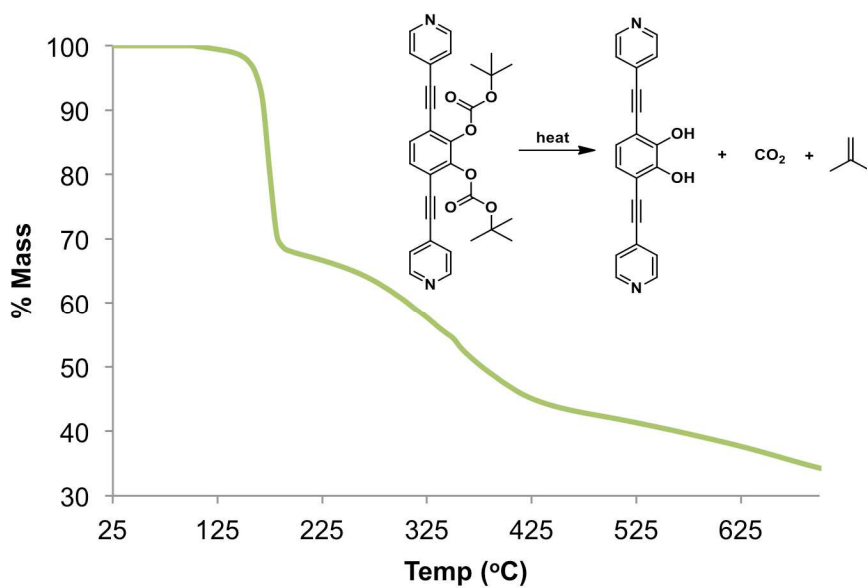


Figure S39. TGA profile of L1_d.

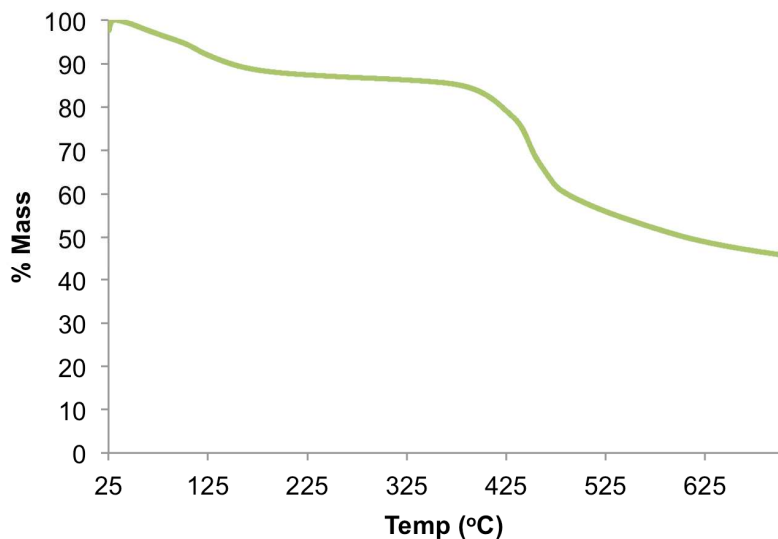


Figure S40. TGA profile of activated **BOC-CatBrO MOF** after solvent exchange to DCM and drying under vacuum at room temperature, showing ~12% mass loss attributed to the BOC groups (expected BOC group mass loss = 15 wt %)

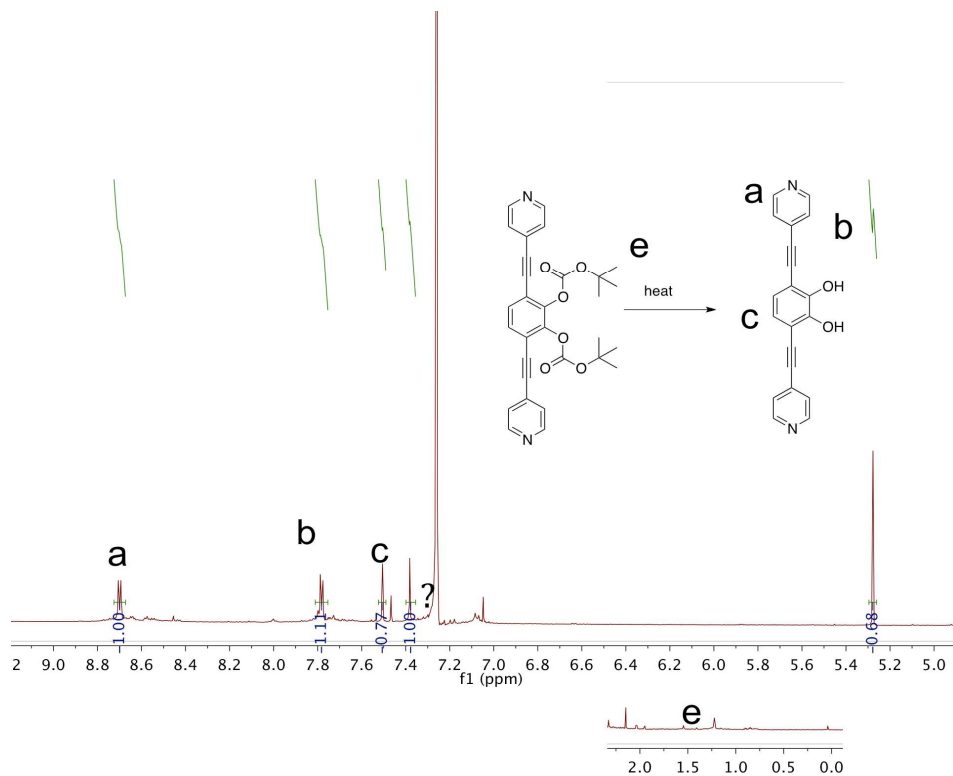


Figure S41. ^1H NMR spectrum of deprotected **BOC-CatBrO-MOF** after activation at 120 °C for 24h. The activated MOF was subjected to DABCO exchange in CDCl_3 prior to NMR analysis.

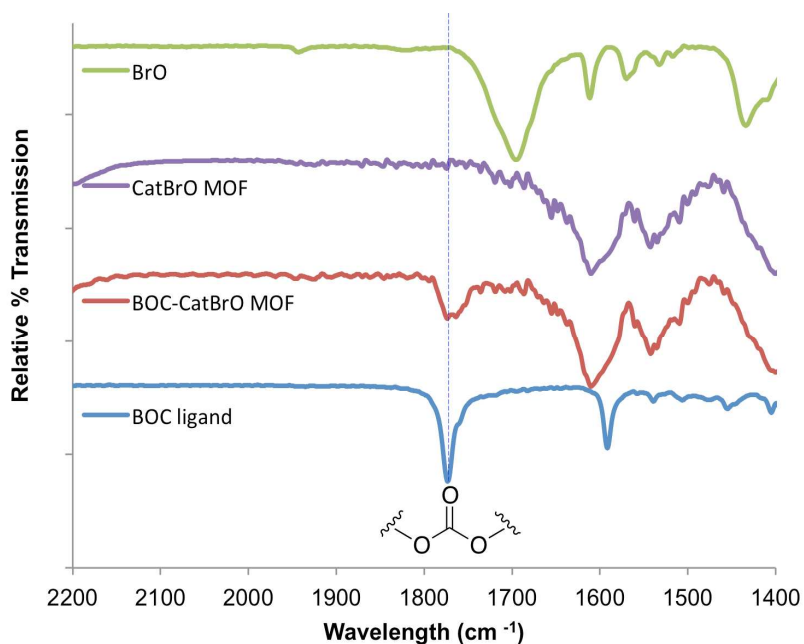


Figure S42. Stacked FT-IR spectra of **L1_d** (blue), **BOC-CatBrO MOF** (red), **CatBrO MOF** (purple), and **L2** (green), highlighting the loss of the BOC group (1775 cm⁻¹) in **CatBrO-MOF**.

Table S4. Vanadium metal loading (as obtained by ICP-OES) for the various solvents used for metallation of **Cat-BrO-MOF** to give **V-CatBrO MOF**

Solvent washes	V/Zn (mol %)*				
	THF	<i>tert</i> -butanol:THF (1/1 v/v)	DMF	MeOH	Dioxane
0 wash	99	3	32	—	—
1 wash	100	3	—	—	—
2 washes	100	NA	17	6	11
DMF, 1 week	30-35				

*Expected V/Zn ratio for 100% metallation of catechols is 50 mol %.

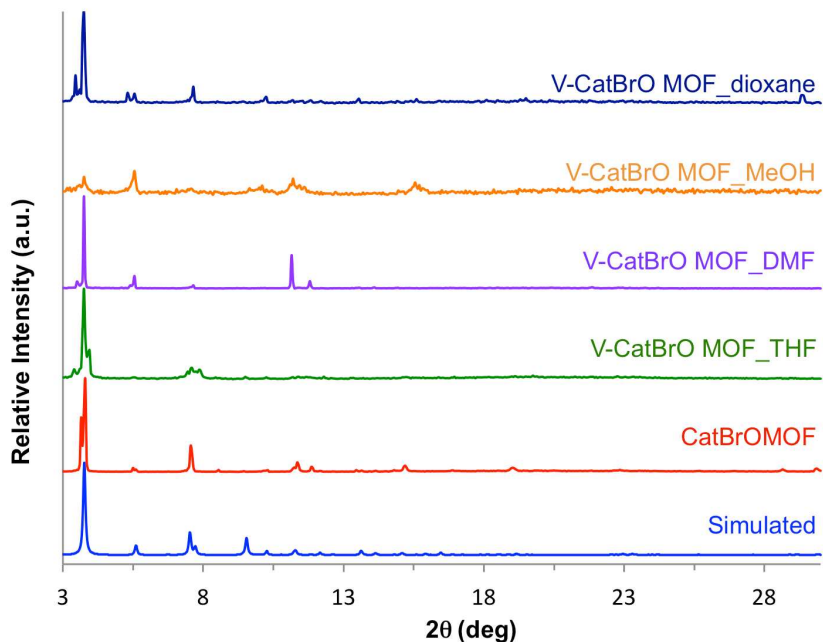


Figure S43. PXRD patterns (bottom to top) of simulated **PG-CatBrO MOF** (blue), **CatBrO MOF** (red), **V-CatBrO MOF** in THF (green), DMF (purple), MeOH (orange), and dioxane (dark blue).

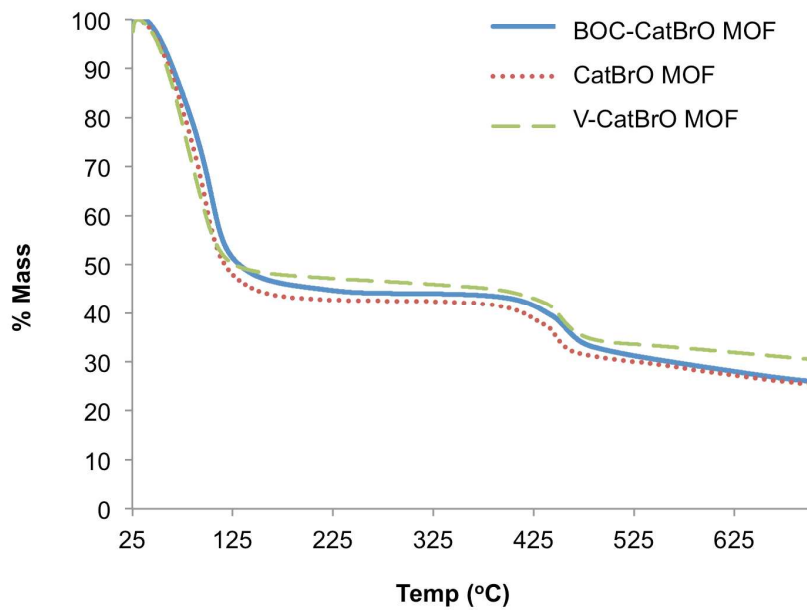


Figure S44. TGA profiles of **BOC-CatBrO-MOF** (solid line), **CatBrO-MOF** (dotted line), and **V-CatBrO-MOF** (dashed line).

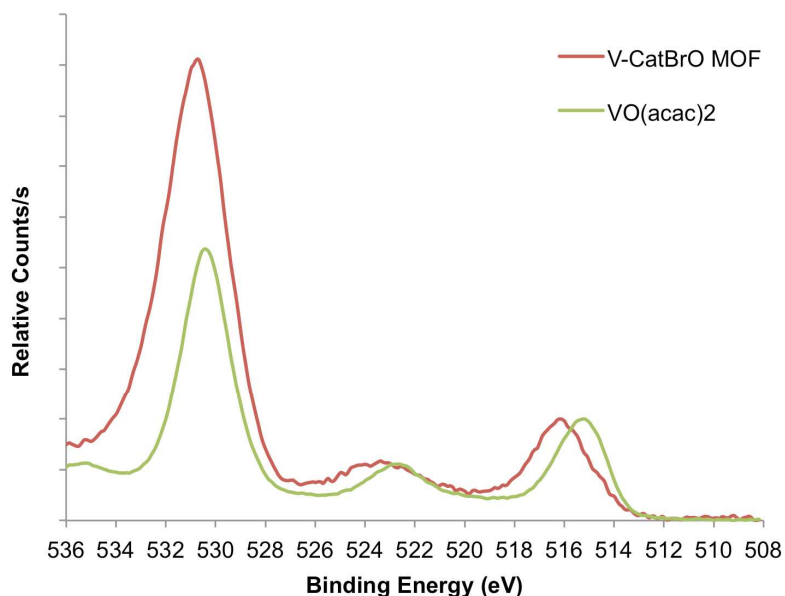


Figure S45. XPS spectra of **V-CatBrO-MOF** (red solid line) and **VO(acac)₂** (green solid line) showing V2p binding energy of 516 and 515 eV, respectively. **V-CatBrO MOF** shows a V2p binding energy of 516 eV, 1 eV shift from the signal (515 eV) for VO(acac)₂, suggesting a change in the coordination environment around the vanadyl ion (possibly due to the binding to catecholate moiety). While 516 eV is slightly less than the 517 eV value expected for V(V) species, it matches well with other literature values for other vanadyl (i.e., V^{IV}) species such as VOSO₄ and VOCl₂.^{S4}

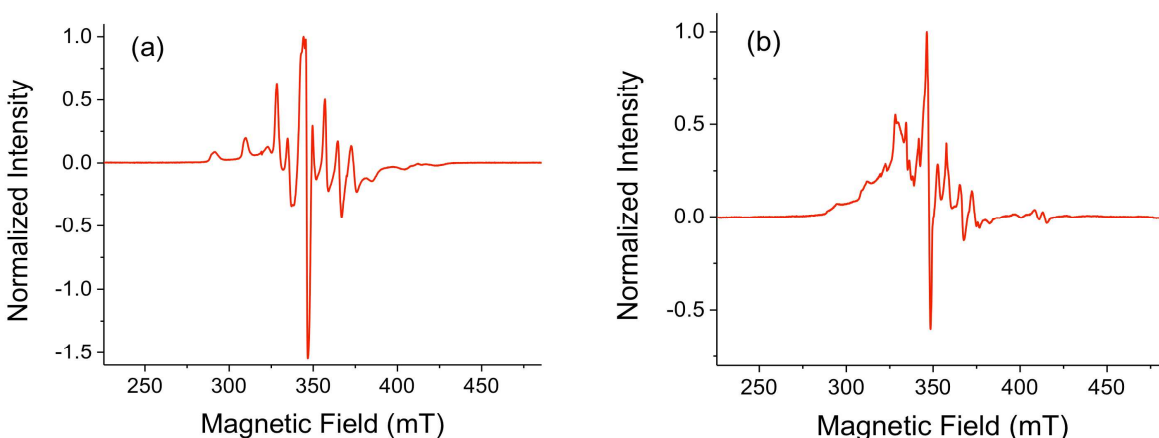


Figure S46. The X-Band CW-EPR spectra of **V-CatBrO MOF**: (a) after solvent-exchanged with dichloromethane and vacuum-dried; (b) soaked in chlorobenzene. Data were collected at 7 K and recorded with a 0.050 mT modulation amplitude. These spectra are comparable to reported spectra of solid-supported vanadyl species.^{S5}

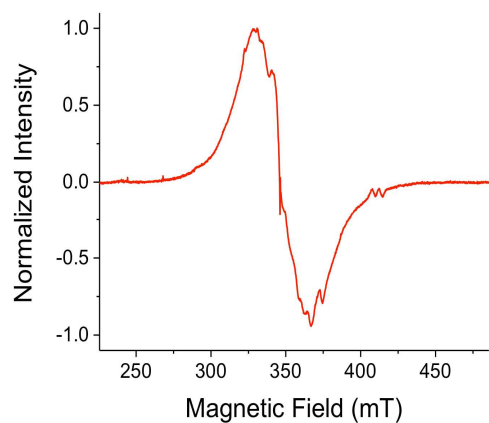


Figure S47. The X-Band CW-EPR spectrum of VO(acac)₂ in chlorobenzene. Data were collected at 7 K and recorded with a 0.050 mT modulation amplitude. This spectrum is comparable to a previously reported spectrum of VO(acac)₂.^{S6}

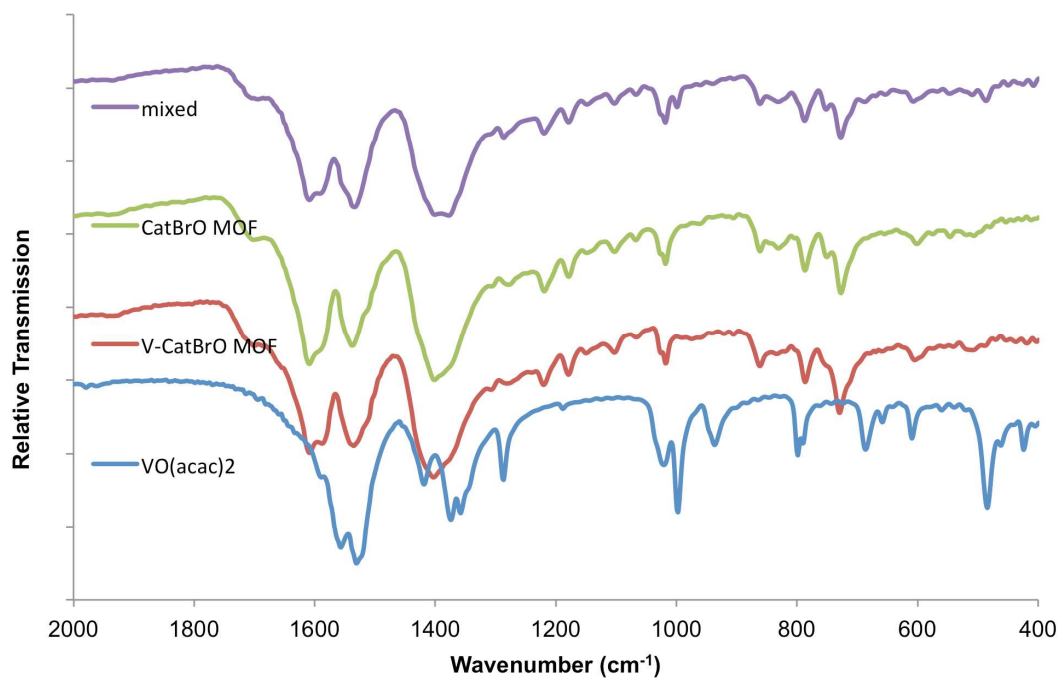


Figure S48 Stacked FT-IR spectra of VO(acac)₂ (blue), V-CatBrO MOF (red), CatBrO MOF (green), and a physical mixture of CatBrO-MOF with 0.35 mol % VO(acac)₂ (purple).

S4. Catalysis-related data

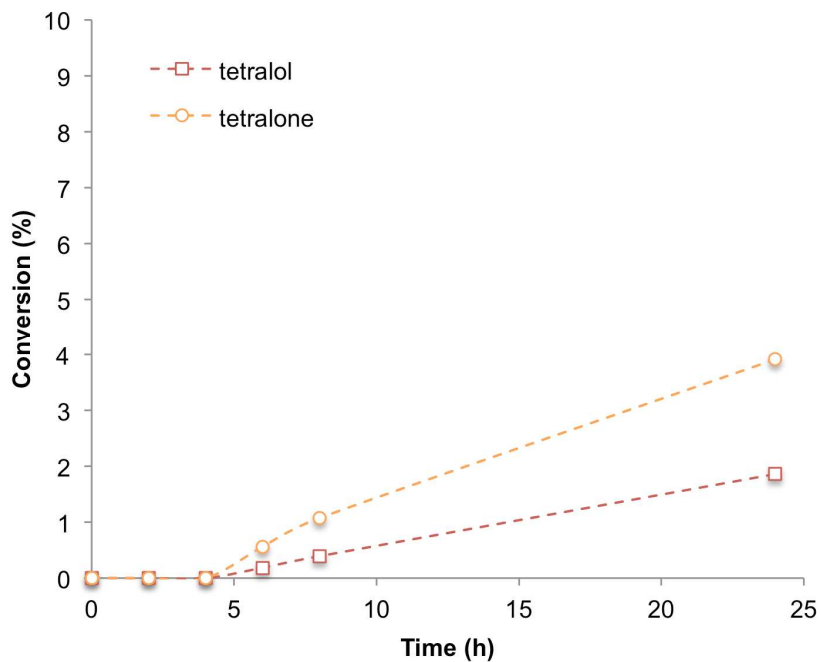


Figure S49. The reaction profile for the oxidation of tetralin into tetralol and tetralone using “metallated” **BOC-CatBrO MOF** (0.07 V/Zn) in the presence of TBHP. Reaction was carried out in chlorobenzene at 50 °C and at a 100:100 molar ratio of tetralin:TBHP. The same molar mass of **BOC-CatBrO MOF** (of MOF and not of V) was used to keep the stoichiometry the same as that in the experiment using **V-CatBrO MOF**. Products designation: tetralone, open orange circles; tetralol, open red squares.

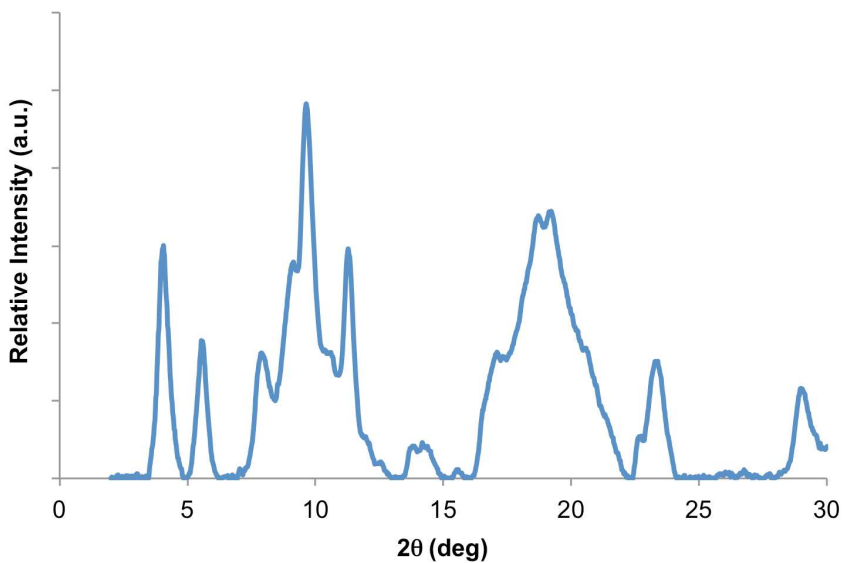


Figure S50. PXRD pattern (obtained using capillary methods) of **V-CatBrO MOF** after catalysis.

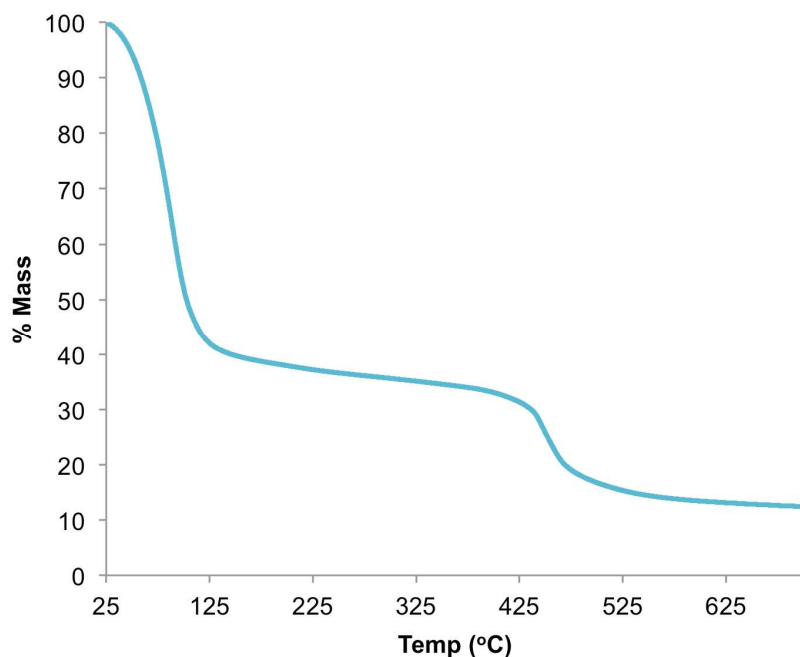


Figure S51. TGA profile of V-CatBrO MOF after catalysis.

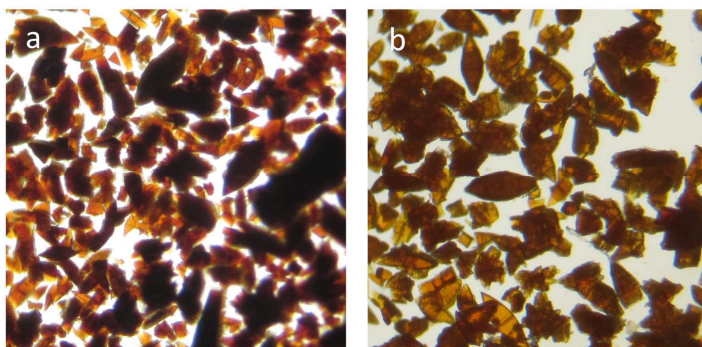


Figure S52. Photographic images (taken under a light microscope) of V-CatBrO MOF before (a) and after (b) benzylic oxidation of tetralin.

S5. References

- S1. Nelson, A. P.; Farha, O. K.; Mulfort, K. L.; Hupp, J. T. *J. Am. Chem. Soc.* **2008**, *131*, 458-460.
- S2. Zhu, Z.; Swager, T. M. *Org. Lett.* **2001**, *3*, 3471-3474.
- S3. Farha, O. K.; Malliakas, C. D.; Kanatzidis, M. G.; Hupp, J. T. *J. Am. Chem. Soc.* **2009**, *132*, 950-952.
- S4. Moulder, J. F.; Stickle, W. F.; Sobol, P. E.; Bomben, K. D. *Handbook of X-ray Photoelectron Spectroscopy*; Physical Electronics, Inc.: Eden Prairie, Minnesota, 1995.
- S5. Segura, Y.; Cool, P. *J. Phys. Chem. B* **2004**, *108*, 19404-19412.
- S6. Öztürk, R.; Gül, A. *Tetrahedron Lett.* **2004**, *45*, 947-949.